Chair of Processing of Composites

Master's Thesis

Evaluation of repairing techniques for damaged natural fiber reinforced composites

Juan Cardenas Velasco

August 2023

AFFIDAVIT

I declare on oath that I wrote this thesis independently, did not use other than the specified sources and aids, and did not otherwise use any unauthorized aids.

I declare that I have read, understood, and complied with the guidelines of the senate of the Montanuniversität Leoben for "Good Scientific Practice".

Furthermore, I declare that the electronic and printed version of the submitted thesis are identical, both, formally and with regard to content.

Date 29.08.2023

Signature Author
Juan Cardenas Velasco

Acknowledgements

I would like to take this opportunity to thank all the members of the Processing of Composites Group who supported me in the preparation of this master's thesis. First and foremost, to the late Univ.-Prof. Dipl.-Ing. Dr.-Ing. Ralf Schledjewski which showed faith in my skills even though I did not excel on the lectures he gave me, he saw a potential in me which I had not realized, and it left a hole in my life by the time of his departure; I will be forever grateful with him.

My special thanks go to MSc Bharath Ravindran for the guidance, supervision, advice and review of all this body of work, as well as the countless discussions during the implementation of this work. This would not have been possible without all of the support.

I would also like to thank Assoc. Prof. Dipl.-Ing. Dr.mont. Ewald Fauster, which with his calm and methodic guidance and resourcefulness in tough times made it possible for me to finish my master thesis on the scheduled time.

In addition, I would like to thank Timotheos Agathocleous, Alexander Hackl and Priv.-Doz. Dr.techn. Beate Oswald-Tranta from the Chair of Automation which offered the equipment from their laboratory and made it possible for me to gather the data required for this thesis.

My absolute thanks also go to the AMASE program for giving me the opportunity to study my master degree away from my country, and furthermore for offering the possibility of having a mobility semester in UPC at Barcelona. AMASE is an experience which I am sure will define my life. To all of the friends that I have made during this experience, who have become my family here in Europe, who had an open ear for me during my studies and thus supported me in achieving my goals, I am forever grateful and I remain forever in your debt.

Finally, I would like to thank my family and my friends in Colombia that gave me their support from afar. It has not been easy starting over, living without you; the support you provided me has been invaluable and gave me the confidence to keep moving ahead despite the complications and the rough times. I will keep on working in making you proud towards achieving my next goal!

Abstract

Fiber reinforced polymer composites employed in industries such as aerospace and automotive, are susceptible to deteriorate over time as a result of impact and moisture absorption. With the widespread use of composite materials, the demand for technologies capable of repairing damaged components rather than replace them has increased in past decade. Additionally, the use of bio-based constituents in composites materials shows an upward trend in the industry. This work will focus on repairing natural fiber reinforced composites, specifically Flax-based composites. For this purpose, two formulations of resin are utilized, a bio-based epoxy resin and a vitrimer resin. Each resin system undergoes a distinct repair technique: injection repair for epoxy-based composites and forming for vitrimer-based ones. The specimens were produced using vacuum assisted resin infusion. The specimens were cut from these plates. A drop weight impact machine was used to damage the specimens in controlled, low-velocity impact test. The repair process for damaged epoxy-based specimens involves resin injection aided by vacuum. The damaged vitrimer-based specimens were formed over a four-hour period within a heating press operating at 160 °C. The efficiency of the repair methods was assessed using active thermography and compression after impact test. Both evaluation techniques demonstrated that the injection repair technique produced favorable results, demonstrating the effectiveness of the repair method for the chosen system. Although the thermographic outcome from the forming technique were positive, the compression properties highlights is ineffectiveness for the chosen natural fiber and vitrimeric system.

1 Content

2 Introduction and objective

Composite materials comprised of a combination of two or more distinct components, are known for their exceptional qualities such high strength-to-weight ratios, durability, thermal stability, and corrosion resistance. This has led to significant interest in these materials across a range of applications including aerospace, automotive, marine, and sports industries.

Despite their outstanding properties, composite materials employed in various sectors that can undergo deterioration over time due to encounters such as impact, heat, and moisture. As a result, failures within composite materials primarily arise from two main sources: material fractures or physical damage. Material fractures encompass the fundamental rupture of the material's structural integrity. Such fractures can originate from various mechanisms, including matrix cracks, debonding between the fiber and matrix, and delamination. Replacing these damaged components involves substantial costs and time for material procurement [1]. Thus, repairing the damaged material emerges as a more economical and time-efficient solution. Furthermore, in the essence of maintaining their performance and extending the lifespan of composites lies in repairing them. Various repairing techniques, such as scarfing and adhesive bonding, have been developed in the past decade.

Initially the damage needs to be addressed. However, assessing the extent of damage in composite materials isn't straightforward through visual inspection alone. Especially, in instances of low-energy impacts, visible surface marks might not be present but they can still cause significant underlying delamination. To detect concealed damage, various nondestructive inspection techniques (NDT) for composites have been developed, including tap testing, ultrasonic inspection, X-ray inspection, and thermography.

Subsequently, the process of repairing composites involves selecting the appropriate repair method [2], and executing the repair using specialized techniques and materials. In this context, having a comprehensive understanding of the

principles governing composite materials and their behavior under varying conditions is imperative to ensure the success of repairs.

2.1 Objective

In this present study, focus revolves around the production and investigation of natural fiber-reinforced composites. Two distinct natural fiber-reinforced composite systems were examined: one based on an epoxy resin while the other based on a vitrimeric functionality. Throughout the study, composite processing properties and techniques will be applied. The investigation will encompass properties related to impact behavior and damage mechanics for these natural fiber-reinforced composites.

The primary objective involves the exploration of repair methods for damaged fiber-reinforced composites. This involves two distinct approaches: Firstly, the repair of damaged natural fiber epoxy-based composites (NF-EP) will involve resin injection. Secondly, damaged natural fiber vitrimeric-based composites (NF-Vi) will undergo a reforming process, utilizing temperature and pressure to activate the vitrimeric self-healing behavior. Subsequently, based on the repair outcomes, an evaluation of the performance of the repaired test specimens will be conducted. This assessment will begin with a nondestructive technique to qualitatively assess the repair results, followed by a destructive technique to quantitatively measure the effectiveness of the repairs.

3 State of the art

3.1 Composite trends

3.1.1 Necessity for repairing

Fiber reinforced polymer composite materials have many uses across all industries, including those in the sports, automotive, marine, and civil infrastructure sectors. This is due to their exceptional properties. Overall, composites' lightweight characteristics aid the automotive industry in cutting carbon emissions, and their high strength characteristics can increase vehicle safety. All of these benefits work together to make composites a desirable material for the automotive and aerospace industry [1].

Because of the high prices and prolonged processing times associated with conventional production methods such as autoclave curing, their application in the automotive industry was limited to small series cars or high-performance sport cars. Resin-transfer-molding (RTM) techniques with lower production costs and lower cycle times have been developed recently for the production of thermoset composites [2].

The growing usage of composite materials in the aerospace and automotive sectors has boosted the need for composites with enhanced lifetime, such as technologies that can repair damaged components rather than replace them with new ones: waste damaged composites may be reduced with a longer composite lifetime, which is helpful to justify the high cost of materials and processing.

3.1.2 Usage of bio-composites

The composite industry is witnessing a notable trend towards utilizing bio-based materials in their compositions. These materials encompass a range of options, including natural fibers such as hemp, flax, jute etc., in combination with partially bio-based or biodegradable resins. This shift is driven by the goal of lowering carbon emissions and establishing a more environmentally sustainable material. Natural fiber offers a renewable and environmentally sustainable alternative to synthetic fiber-based conventional composites used in various applications because of their

easy decomposition, lightweight, high specific mechanical properties, less tool wear during processing [3]. Within this context, natural fiber-reinforced bio-composites have gathered significant attention as a viable, long-term alternative to traditional fiberglass composites across various applications within the composite field [3]. Notably, sectors such as sports, automotive, and packaging, as previously mentioned, are expected to constitute the primary target market for these innovative natural fiber-reinforced bio-composites.

In terms of strength and stiffness of wide range of natural fiber, flax stands out as one of the most promising. Interestingly, comparisons often highlight that glass fiber reinforced plastics and composites based on flax exhibit comparable specific strengths [4]. This intriguing similarity suggests the potential to substitute glass fibers with flax fibers in the fabrication of materials, leading to enhanced structural stability in the final product.

3.2 Load and impact damage on composites

Composite structures may experience impact loads over the course of their service life from dropped tools, collisions with loading and unloading fixtures, cargo, or even from ballast itself. These impact occurrences have the potential to cause internal damage that significantly reduces the composite's remaining mechanical properties.

In general, there can be four different types of impact velocity categories, namely low, high, ballistic and hypervelocity [5]. While low velocity impacts (< 11 m/s) may occur through dropped tools during maintenance operations, high velocity impacts (> 11 m/s) are usually performed through bird strikes, hail or runway debris hitting the fuselage during landing or starting operations. Ballistic impacts, on the other hand, are typically a concern for military applications because they are typically caused by ballistic impacts (> 500 m/s). Finally, the hypervelocity impacts (> 2000 m/s), typically brought on by objects slamming into satellites or spacecraft.

3.2.1 Low impact damage modes in composites

Four major modes of failure can be identified for low velocity impacts, due to the heterogeneous and anisotropic nature of fibre reinforced plastic composites [5]:

1. Matrix failure – damages in the form of matrix cracking and interface bonding between the fibre and the matrix, usually oriented in a plane parallel to the fibre direction in unidirectional layers
2. Delamination – a crack that runs in the resin-rich area between plies with different fibre orientation as a result of the bending mismatch coefficient between the two adjacent laminates
3. Fibre failure – generally occurs much later in the fracture process than matrix failure and delamination and before the catastrophic penetration mode. High local stresses and indentation effects of shear forces as well as high bending stresses on the non-impacted face, caused by the penetrators impact lead to fibre failure.
4. Penetration – a macroscopic mode of failure that occurs when the fibre failure enables the penetrator to completely penetrate the laminate structure.

Figure 1 shows the typical impact damage effects on a composite structure, including transverse cracks, fibre breakage as well as delamination.
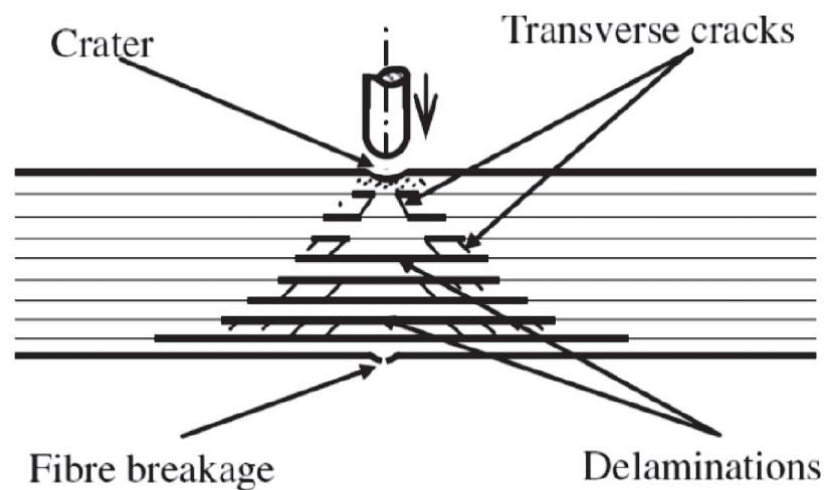

Figure 1: Typical Iimpact damage effects on a composite structure [6]

Delaminated plies do not have a large effect on the tension strength of the overall composite structure, but can significantly diminish the composites compression strength, not only locally but also on a global scale, since they have a lower buckling resistance compared to solidly bonded plies.

While for metallic structures the damage and failure characteristics are relatively well understood, since their in-service damage and failure occurs mostly due to the propagation of fatigue cracks under cyclic loading. In contrast, a number of factors can be responsible for damage and structural failure in composite materials. In addition to the fact that composites are typically susceptible to hidden or hardly noticeable low-velocity impact damage, which can dramatically reduce structural strength, the failure modes under compression and tension differ significantly from one another [6]. Shear, tension, and compression are the three main failure modes for composites.

Since the composite material consists of multiple layers with different orientations, especially in aircraft applications, the projection of global stresses on the main directions of the laminate varies from ply to ply as the load increases. The various stresses in the laminate also change, and failure values can be reached in a given composite in a principal direction without an overall failure of the structure.

In general, this means that the evolution of the failure characteristic of a composite laminate is a progressive phenomenon, while it can be subcritical for a time it can eventually lead to a catastrophic damage state [6].

3.3 Repair methods

For repairing damaged fiber-reinforced composites, several techniques are employed but the most extensively used methods are: scarf repair (SR) and injection repair (IR) [2]. These techniques are discussed in the following section because they are long-term fixes that can also be applied to parts that are relevant to automotive application, which is the largest market for composites.

3.3.1 Scarf repair

Due to its low cost and ease of use, scarf repair is one of the most popular repair methods for all types of FRP. SR comes in two main varieties: stepped scarf repair and tapered scarf repair. In Figure 2 these two methods of SR are depicted. For SR, there are typically five fundamental steps. The damaged area must first be localized using NDT techniques. The damaged area must then have several layers removed from it. A taper ratio of 50:1 is suggested for the repair depending on the

type of material, layer structure, and adhesive. The removal of the layers can be achieved with milling, laser ablation or abrasive water jet cutting. The damaged part must be cleaned after cutting, and the surface energy must be increased. This is required to get the repair patches to adhere well to the damaged area. There are a variety of techniques available to increase surface energy, including grinding, sandblasting, plasma or laser surface treatment, and more.
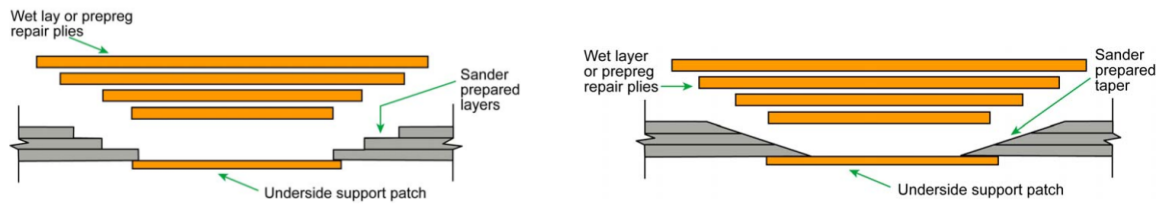

Figure 2: Scarf repair types: Stepped scarf repair (left) and tapered scarf repair (right) [7]

The repair patches can be applied after the surface has been cleaned. For the repair, prepreg material or wet lamination can be used; prepreg material must be kept at a low temperature to prevent premature curing, which makes it more expensive and challenging to store [7].

3.3.2 Injection repair

As compared to more intricate SR techniques, the preparation of the damaged surface structure for IR is less demanding, making the process simpler to execute. If there is a chance that the part might be contaminated, IR should be avoided. Furthermore, if any contamination occurred during the impact, the fractured surface needs to be thoroughly cleaned. The scarf repair method can lead to changes in the material properties and overall weight of the structure. Due to these potential alterations, the injection repair technique is often regarded as a more favorable option. A hole known as an injection hole (IH) and typically 2 to 6 vent holes (VH) around the injection hole are drilled in order to access all cracks in the damaged parts [8, 9]. To prevent damaging the surrounding areas, pulling out fibers, or damaging them, the holes must be carefully drilled.

Moreover, because the holes disrupt the force flux of the fibers, a weakening of the structure cannot entirely be prevented. The quality of the holes is influenced by the cutting parameters, tool geometry, and material [2]. Polymeric composites are most

frequently drilled with tungsten carbide drills [10]. In general, higher rotation speeds (>600 rpm) and lower feed rates (0.25 mm/rev) are more beneficial for minimizing damage [2, 10, 11].
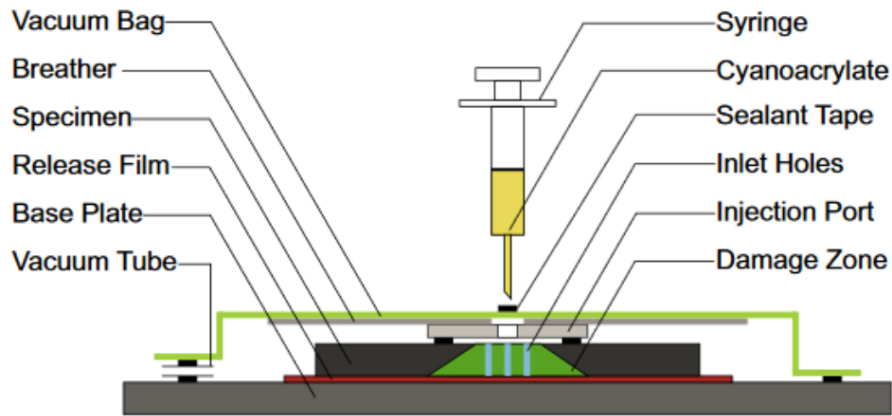

Figure 3: Injection repair setup, depicting vacuum bag puncture [12]

Slattery et al.'s [12] method involved injecting fluid through a vacuum bag using a syringe. Figure 3 depicts the configuration. The composite component is set atop a release agent-coated steel base plate. A hole is located in the middle of the polycarbonate injection port. The top of the specimen is covered with a breather sheet. The center of the breather is hollow. To create vacuum, a vacuum bag and sealant tape are used. Additionally, resin is applied in a pool to the sealant tape. A needle with a 1 mm diameter is attached to the syringe, and it pierces both the vacuum bag and the sealant tape. The resin inside the needle is pulled into the center hole in the composite part after the vacuum bag has been punctured [12].

3.4 Vacuum assisted resin infusion

Vacuum Assisted Resin Infusion, commonly known as VARI, is a composite manufacturing technique used to fabricate durable and lightweight structures. It is widely employed in industries such as aerospace, automotive, marine, and wind energy, where the demand for high-performance and cost-effective composite materials is dominant. In VARI, a dry preform, typically consisting of reinforcing fibers (such as carbon, glass, aramid or natural) is placed on top of a mold [13]. The

preform is carefully arranged to achieve the desired fiber orientation and laminate architecture. A flexible vacuum bag is then placed over the preform and sealed around the mold perimeter. Next, a liquid resin system is introduced into the mold. The resin is carefully selected to match the specific requirements of the application, such as mechanical properties, curing characteristics, and environmental resistance. The resin is typically low viscosity, allowing it to flow through the preform and impregnate the dry fibers.

Under the influence of the vacuum pressure, the resin flows through the preform, displacing any trapped air or excess resin. This process is often referred to as resin infusion. The vacuum also helps to consolidate the laminate by applying uniform pressure, ensuring complete wet-out of the fibers and minimizing voids.

Once the resin has fully infiltrated the preform, the curing process begins. This can be achieved through various methods, such as the application of heat, catalysts, or UV light, depending on the resin system used. The curing process transforms the liquid resin into a solid matrix, binding the fibers together and forming a robust composite structure [13].

3.5 Vitrimer-based composites background

In order to understand the potential impact and importance of a possible self-healing vitrimer composite, it is essential to explore into basic definition of vitrimer and its particular chemistry.

3.5.1 Vitrimer Chemistry

Extensive research has been conducted in recent years on vitrimeric polymers due to their promising properties. The term was first introduced and defined by Ludwik Leibler's research group in 2011. Leibler et al. investigated a polymeric network containing dynamic covalent bonds, known as Covalent Adaptable Networks (CAN's), which can undergo exchange reactions at high temperature [14].

Dynamic covalent bonds can engage in both associative and dissociative exchange reactions. The associative exchange reaction involves the formation of a new linkage followed by the breaking of another bond, leading to an increased linkage density in the intermediate stage. However, due to the rapid succession of these

reactions, the effect on crosslink density can be disregarded, assuming it remains constant throughout the process [15, 16].

In contrast, a bond is broken in the first phase of a dissociative exchange, which results in a reduction in the number of linkages, and then a new coupling is formed, which leads to an increase in the number of linkages [15–17]. If the equilibrium shifts, this behavior may result in a drop in crosslink density or even complete depolymerization [18].

Vitrimers are systems that have a constant number of bonds from the fully cured state to the point of decomposition [18, 19]. Leibler et al. made the first step towards a constant crosslinking density, and this work is based on CANs by transesterification between ester and alcohol in an epoxy matrix [14]. The Arrhenius dependence of viscosity on temperature above the vitrimer transition temperature (Tv), also known as the "topology freezing temperature", is another characteristic that defines vitrimers [14, 17]. By definition, Tv is reached when the viscosity of the system equals 10^{12} Pa s [14]. Below this temperature vitrimers behave like duromers, above Tv they exhibit properties of a viscoelastic fluid [15, 17, 20]. However, unlike the glass transition temperature (Tg), Tv tends to extend over a broader temperature range. In addition, Tv represents a solid-solid transition, whereas the glass transition is a liquid-solid transition [11]

Whether Tv is above or below Tg is important for the thermomechanical characteristics of vitrimers. One or the other variant may be interesting to achieve the desired properties depending on the application [19, 20]. Exchange reactions are already occurring between Tg and Tv, but their velocity is too slow to permit macroscopic flow. If Tv is a temperature lower than Tg, which means that the activation energy for the exchange reaction is comparatively low, the glass transition temperature determines the point above which viscoelastic flow is possible. Below Tg, exchange reactions are hindered by low chain mobility. Similar circumstances apply to semi-crystalline vitrimers; if Tg is below Tv, the material behaves elastically in the range between the two temperatures, and over Tv, the material behaves viscoelastically in accordance with the Arrhenius approach [19, 20].

Leibler et al. were able to demonstrate that the amount of catalyst added can affect Tv's position in their more recent work on vitrimeric systems. A higher concentration of zinc acetate as a transesterification catalyst lowers the viscosity and vitrimer transition temperature in an epoxy matrix of Bisphenol-A-Diglycidyl ether (DGEBA) and tri- or dicarboxylic acid [19, 20].

Both "crosslinking of thermoplastics" and "polymerization of multifunctional monomers" can be used to create vitrimers. In each case, there are three different ways to introduce a dynamic covalent bond. The dynamic bond can be introduced:

1. From an existing network during polymerization by changing the formulation or adding a catalyst
2. It can already be present in one of the monomers,
3. It can be formed directly during the network formation process.
4. It is already present in the molecule that is responsible for crosslinking

A thermoplastic must have its macromolecular chains crosslinked to become a vitrimeric polymer system. Here, the dynamic bond may either be present in the initial polymer or may be specifically added during synthesis, and the vitrimer function is achieved through crosslinking with the help of a multifunctional molecule [18, 19].

As previously mentioned, the first vitrimers were created involving zinc acetate as catalyst to transesterify ester and alcohol in an epoxy matrix [14]. In the field of vitrimers, zinc-based catalysts are frequently used because they provide system stability at high temperature. However, other catalysts have also been used successfully for the transesterification reaction, such as Triazabicyclodecene (TBD) or Triphenylphosphine (TPP) [15, 17].

3.5.2 Vitrimeric-Based composites materials

Numerous experiments have already been conducted to examine the potential of vitrimeric matrix systems. On the one hand, transesterification was used to show the self-healing or weldability of a vitrimeric epoxy resin based on soybean oil and aqueous citric acid solution on pure resin specimens [21]. Here after forming at 160 °C for 60 and 120 minutes, respectively, the damaged specimens were able to

achieve comparable stress and strain to failure values in tensile shear tests compared to the undamaged specimens.

Other work has been carried out on fabric or fiber-reinforced test specimens in order to integrate vitrimers in a composite system. Depending on the resin system, various conventional composite manufacturing processes are suitable for this purpose. In the mentioned works on fiber-reinforced vitrimers, the composites were produced either by Resin Transfer Molding (RTM) [22] or hand lay-up [20, 22].

In the study conducted by Stryzek [23], two vitrimeric systems were employed to produce composite plates through the VARI method. The first resin system comprised epoxidized linseed oil, glutaric anhydride, and TBD as a catalyst. The second system consisted of Pripol, DGEBA, and TBD. However, the latter system encountered challenges due to the elevated viscosity of Pripol, making its processing using this approach problematic.

3.6 Forming of vitrimer-based composites

Forming, a procedure primarily associated with thermoplastics in the past, has found a new realm of application with the advent of vitrimers. This innovative class of materials offers the prospect of integrating the flexible shaping abilities inherent to thermoplastics with the robust mechanical properties, characteristic of thermosets. This integration of attributes opens up intriguing possibilities for manufacturing. The ability to form vitrimers has already been validated through various research endeavors. [20, 22–24].

In the research work of Ruiz de Luzuriaga et al [15], the vitrimer function was highlighted by performing the same experiment also on a non-vitrimer reference resin system, which is broken during the forming process. Weidmann et al. [24] go further and examine the specific reshaping mechanisms that were observed, while Denissen et al. [20] also demonstrate in their work the possibility of reshaping the vitrimers used.

Five mechanisms are listed as typical forming mechanisms: interlaminar shear, matrix penetration, ply displacement (also known as "ply-sliding"), fiber buckling, and fabric stretching. To achieve good forming quality, ply-sliding, fabric stretching,

and interlaminar shear are essential. Inadequate performance of these mechanisms can lead to flaws such as fiber buckling or wrinkles. Matrix impregnation occurs mainly at low viscosity matrix and results in matrix-rich zones on the outside of radii. Wrinkling, on the other hand, often occurs when the matrix viscosity is too high [23]. In the work of Weidmann et al. the occurrence of forming mechanisms was considered in a thermoforming test where 8 layers of carbon fiber were formed in an omega profile [23, 24]. In the test specimens, holes were drilled to see if ply-sliding took place. By looking at the lateral cross-section, it was possible to determine the displacement of the plies on the side surfaces of the omega after it had formed [24].

In Stryzek's study, the omega profile was employed to investigate the impacts of temperature, forming duration, and number of layer count on a vitrimer-based composite. Notably, a significant finding was the unexpected impact of the number of layers due to fiber damage occurring within the inner curves of the omega profile when utilizing multiple layers. The experiments conducted underscored the practicality of shaping vitrimer composites with a commendable level of accuracy [23].

4 Materials and experimental methods

4.1 Textile for fiber reinforcing structure

For the fabrication of the composite plates, there is a specific emphasis on integrating a reinforcing structure derived from natural fibers. The primary objective is to employ a natural fiber material that offers flexibility during the shaping process and facilitate manual handling. Also, the selected natural fiber must possess a substantial areal density of no less than 300 g/m2 which enables to achieve a predetermined panel thickness and minimizing the number of layers required to achieve the target specifications.

In this context, addressing the prerequisites and thorough evaluation of available options, the Flax fiber Amplitex 5042 supplied by Bcomp Ltd, Fribourg, Switzerland, was selected as the optimal choice due to material's characteristic and its widespread market availability. The selected material, is a woven fabric featuring a balanced 4x4 twill weave pattern incorporating yarn with a tex count of 500, no twist. The 4x4 twill weave imparts a balanced distribution of strength and flexibility to the material. This weave pattern is instrumental in enhancing the material's load-bearing capacity and overall durability, thereby contributing to the mechanical integrity of the composite plates.

4.2 Resin systems for composite plates

In the context of the present study, a focus on sustainable matrix systems is promoted. To address this, the research will involve the utilization of two distinct resin systems: epoxy-based and vitrimer-based.

4.2.1 Resin selection for epoxy-based system

To characterize the repair approach of a sustainable matrix system, a partially bio-based epoxy resin Epinal b.poxy IR78.31 (37.58 % of bio-based resin content) and Epinal IH77.11 amine hardener supplied by bto-epoxy GmbH (Amstetten, Austria) were selected as the primary resin system. The resin and hardener were mixed in the ratio of 100:25 by weight.

4.2.2 Resin selection for vitrimer-based system

In order to investigate and characterize the repair methodology for vitrimer-based reinforced composite, a comprehensive mixture of three substance will be used: These substances include the resin Epinal NFL 10.20 -A4.00, epoxidized linseed oil (ELSO) and the catalyst TBD (*Triazabicyclodecene*), specifically 1,5,7-Triazabicyclo [4.4.0] dec-5-ene supplied by bto-epoxy GmbH (Amstetten, Austria), while the hardener Glutaric anhydride from Sigma-Aldrich Handels GmbH (Vienna, Austria) [25] will be used into the mixture. TBD is a proven and effective catalyst in facilitating transesterification reactions [15, 26]. Its inclusion in the mixture is key for the formation of Covalent Adaptable Networks within the matrix , a crucial aspect of the repair approach [17]. The resin and curing agents are mixed in a 100:34 weight ratio, with 10 % of TBD (by weight) [23]. This precise formulation and the catalytic function of TBD are integral to achieving the targeted matrix characteristics and repair capabilities.

4.3 Manufacture of composite plates

VARI was used to manufacture both the epoxy-based and vitrimer-based composite plates from which the test specimens were extracted. To achieve this, distinct sets of plates were prepared. Specifically, for the epoxy-based plates, three plates measuring 800 mm x 350 mm were created. In the case of the vitrimer-based plates, two plates sized at 550 mm x 350 mm were fabricated.

4.3.1 Materials for manufacturing of composite plates

The following materials were used to create both the epoxy-based and the vitrimer-based fiber reinforced composite plates:

- Electric heating plate Hillesheim GmbH (Waghäusel, Germany)
- Vacuum pump TRIVAC Leybold GmbH (Cologne, Germany)
- Chemlease® 75 EZ Release Agent Chem-Trend GmbH (Maisach, Germany)
- Oven Model FDL 115 Binder GmbH (Frankfurt, Germany)
- Release peel ply
- Flowing media
- Vacuum bag

- Vacuum hose (5 mm in diameter)
- Valves and clamps
- Sealant tape
- Distribution channels

Furthermore, the Flax fiber perform was cut using an electronic cutter type G3 Zünd Systemtechnik AG (Altstätten, Germany). Subsequent to the cutting process, the flax fabric was precisely organized into groups consisting of six layers each. This assembling was carried out to facilitate smoother handling and preparation for subsequent stages.

4.3.2 Setup of VARI manufacturing

Prior to the manufacturing, the preform were subjected to a temperature at 120 °C within oven for at least 30 minutes. This step was undertaken with the primary objective of effectively minimizing the moisture content already present within the fibers. [27, 28].
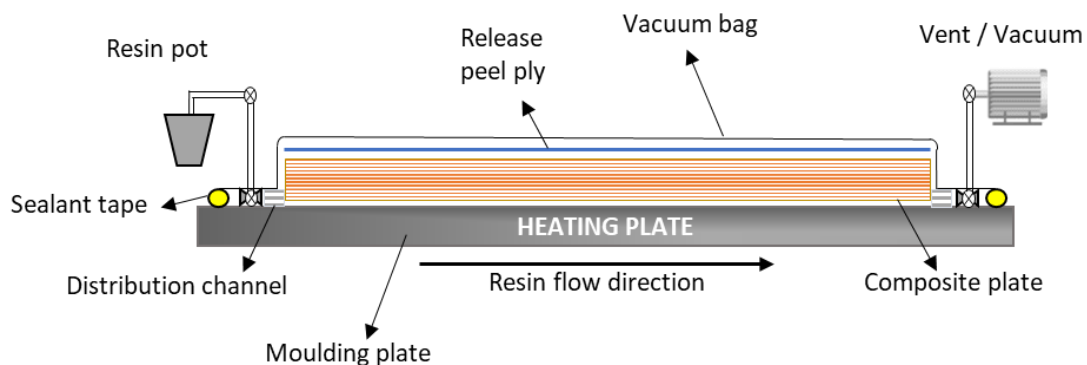

Figure 4: Schematic of VARI composite plate manufacturing [29]

The heating plate's surface is subjected to a thorough cleaning using isopropanol which effectively removes dirt or grease residue. Following this, a coating of release agent, Chemlease® 75 EZ was subsequently applied. The heating plate was then preheated to a temperature of 60 °C. The complete setup for the VARI manufacturing process is illustrated in Figure 4: To begin, the preform consisting of six layers of flax fabric were strategically positioned atop the heating plate. Subsequently, the release peel ply was laid over the perform, and in the case of vitrimer-Based resin, the flow media ply was added on top. The distribution channels

were carefully positioned close to the preform. Additionally, the resin inlet and outlet tubes were appropriately situated as well [29].

Following the setup, the preform is sealed with a vacuum bag with the help of the sealant tape. A vacuum test is performed to the system to identify any leaks; thus, leaks can be rectified by reshaping the sealant tape which is depicted in Figure 5.
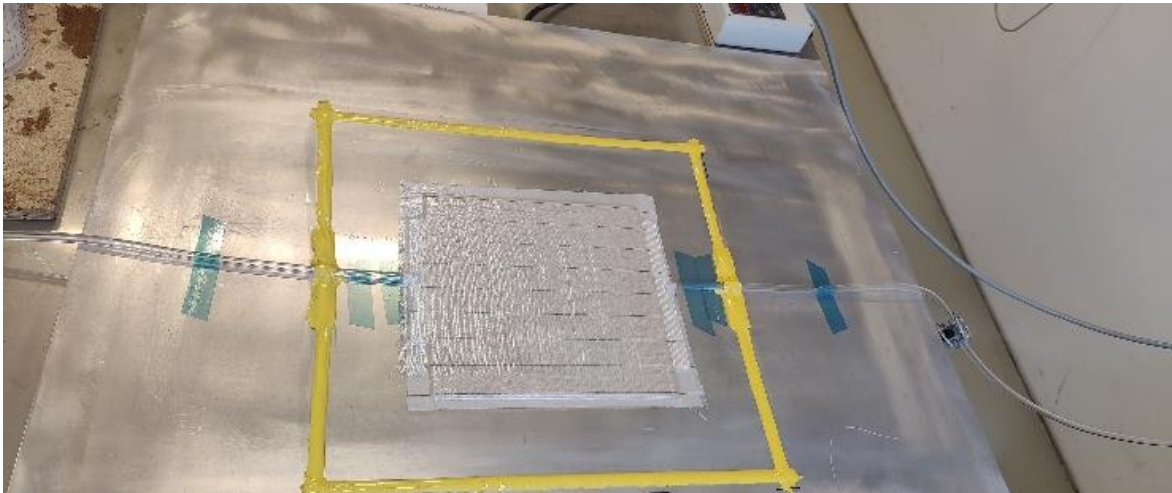

Figure 5: Setup of VARI composite plate manufacturing

Subsequently, the heating plate is subjected to a specific temperature corresponding to the matrix system being utilized. For the NF-EP plates, the heating plate is set at a temperature of 80 °C. Conversely, for the NF-Vi plates, the heating plate's temperature is elevated to 120 °C [23].

4.3.3 Epoxy-based resin preparation

The epoxy matrix consists of two components, which are individually measured and combined in a 100:25 by weight ratio of resin to hardener. The amount of resin to be measured was determined as 20 % more than the weight of the fibers after they had been in the oven for a minimum of 30 minutes. This weight is referred to as the "dry fiber weight."

The two components were blended together at room temperature using a wooden stick in a polypropylene beaker known as the "resin pot." Following mixing, the resin mixture is subjected to degassing using vacuum prior to the infusion process to remove any trapped air bubbles or gases from the mixture.

4.3.4 Vitrimer-based resin preparation

The preparation method for the vitrimer-based resin underwent testing, and the specific setup discussed here represents the most effective outcome from the tested approaches. Further details about this preparation will be provided in section 5.1.

For the preparation, the ELSO resin and the hardener glutaric anhydride were placed in separate beakers and heated inside an oven at a temperature of 80 °C for a duration of 30 minutes. During this heating process, the glutaric anhydride, which was initially a yellow-colored powder at room temperature, transformed into a liquid state. This transformation was carried out to facilitate more efficient mixing.

After heating, the preheated ELSO resin was transferred to a heated plate, and a magnetic stirrer was inserted into the beaker. The resin was initially mixed with the catalyst TBD and subjected to degassing for a period of 5 minutes. Following this, the liquid glutaric anhydride was added to the mixture, and the stirring process continued for an additional 5 minutes. Subsequently, the mixture engaged in an additional degassing step lasting 1 minute, just before the infusion process.

4.3.5 Resin infusion

The VARI process involves utilizing a pressure gradient to facilitate the infusion. The resin moves from a container operating at atmospheric pressure towards a lower pressure zone generated by a vacuum pump. The inlet tube has been positioned within the resin pot. To initiate the infusion process, it's necessary to open both the inlet and outlet valves.

Once the infusion process initiated, the resin will establish a flow front as depicted in Figure 6a. Initially the resin expands perpendicular to its path and subsequently gradually advancing towards the side connected to the vacuum. In the case of the vitrimer-based resin, the flowing medium was applied over the release peel ply. This medium creates a pathway of reduced resistance, facilitating the resin's longitudinal flow across the plate. This approach enhances impregnation, reducing infusion time, given that the vitrimer remains relatively viscous at 80 °C compared to the epoxy resin at room temperature. Conversely, the epoxy resin did not require a flowing

media layer due to its lower viscosity. Flow channels for resin movement were provided by the twill flax, as reported [30].
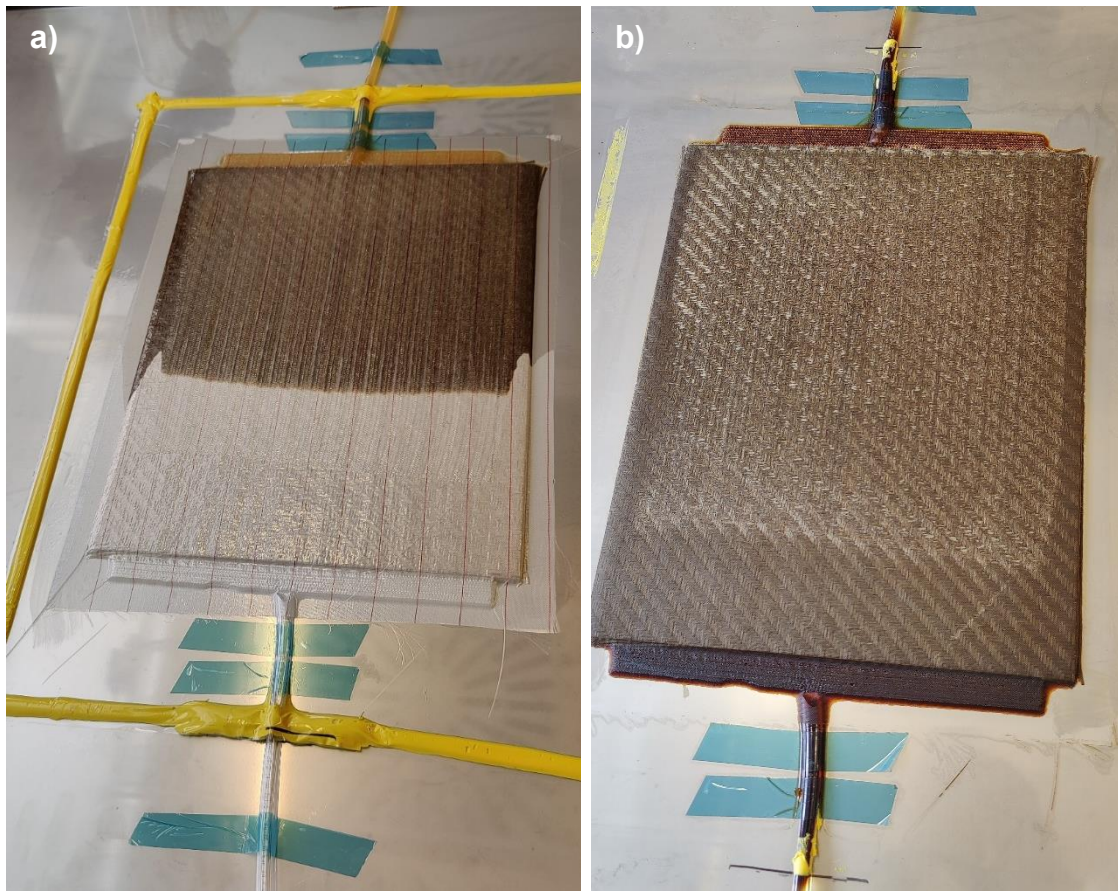

Figure 6: VARI process

a) Resin flow front in the middle of process. b) Cured fiber reinforced plate in pre-demolding stage

The infusion process concludes upon resin arrival at the outlet tube. Simultaneous closure of the inlet and outlet valves follows, ensuring the maintenance of compaction generated by the vacuum.

Following this stage, the curing process take place based on the specific matrix used. The chosen epoxy resin necessitates 3 hours of curing at 60 °C, whereas the vitrimer resin demands 20 hours at 120 °C. Upon completion of the curing process, consumables such as the vacuum bag, release peel ply, and flow medium are removed from the heating plate, leaving the fiber-reinforced composite as depicted in Figure 6b. This composite is now prepared for meticulous demolding, a step facilitated by the use of a wooden tool.

In Table 1 an overview of the key different described process parameters is presented for both resin systems.

Table 1: Overview of material process for NF-EP and NF-Vi plates

	NF-EP	NF-Vi
Composite plate components	• Flax fiber, six layers • Epoxy resin • Amine hardener	• Flax fiber, six layers • ELSO • Glutaric anhydride • TBD
Preheating	No	ELSO and glutaric anhydride during 30 minutes at 80 °C
Flowing media	No	Yes
Curing time	3 hours	20 hours
Curing temperature	60 °C	120 °C

4.4 Specimen preparation

The specimens to be impacted were cut in the same dimensions for both the epoxy-based and vitrimer-based plates, 150 mm x 100 mm, as this is an standard dimension for drop impact test and compression after impact, as described in ASTM D7136 and ASTM D7137 [31, 32].

The plates were cut with the help of a circular table stainless steel saw. From them, the three epoxy-based (800 mm x 350 mm) yielded 14 specimens each, and for the vitrimer-based two plates (550 mm x 350 mm) 8 specimens were taken for each.

4.5 Flash infrared thermography setup

Various techniques exist for identifying flaws in composite materials following an impact. Visual inspection serves as an initial assessment, gauging surface damage

to ascertain the potential severity of defects. Although this method is quick and doesn't require specialized equipment, its accuracy is limited, necessitating supplementary approaches. Numerous non-destructive testing (NDT) methods are available for examining composite materials, including ultrasonic testing, X-radiography, thermography, eddy current testing, and acoustic emissions.

The central focus of this project is to evaluate the repair method through the utilization of non-destructive techniques (NDT). For addressing non-visible impact damage, such as that induced by drop weight impact, the commonly employed technique of flash infrared thermography is employed [13].
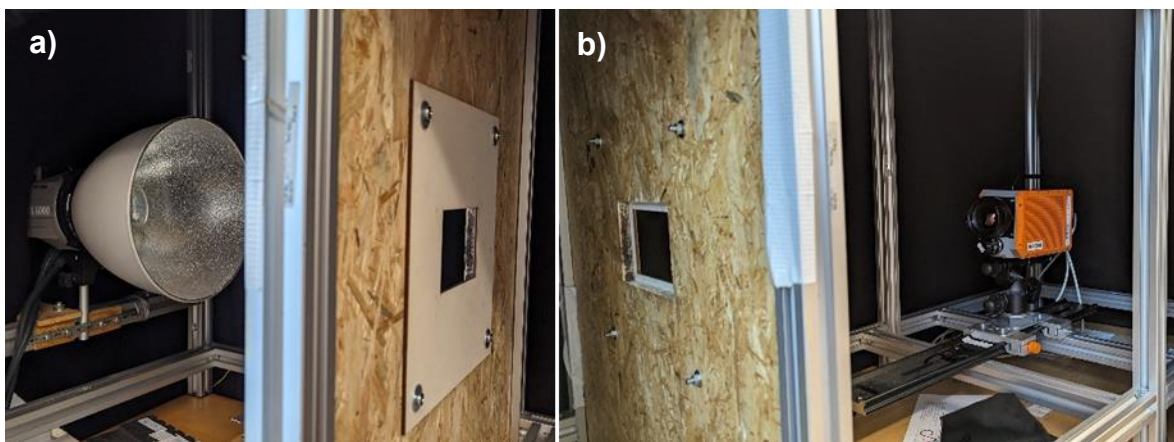
Figure 7: Flash thermography setup.
a) Flash lamp next to sample holder, b) IR camera next to sample holder

Infrared thermography relies on a heat source, here represented by a flash lamp, in combination with an IR camera to provide thermal images of the specimens. In this configuration, a transmission setup is employed. The flash lamp is positioned at a distance of 360 mm from the specimen as shown in Figure 7a, while the IR camera is situated at a distance of 630 mm as depicted in Figure 7b. Images are captured over a 100-second interval at a frequency of 5 Hz. Subsequently, all images are normalized using an averaging code in MATLAB, referencing the maximum temperature. This process generates the resulting images, which will be presented in subsequent stages.

The imaging process involves capturing images of the assessed specimens prior to and after the drop weight impact. Additionally, a third set of images is captured subsequent to employing the repair method.

4.6 Weight drop impact setup

The drop weight impact were conducted to the selected specimens following the ASTM D7136 [31], a standard test method for drop tower impact testing of a composite. The instrument used were the drop tower CEAST 9350 (Instron, UK) with a hemispherical impactor of diameter 20 mm. The machine is equipped with a force sensor that activates as soon as the impact has been done to prevent a rebound impact.
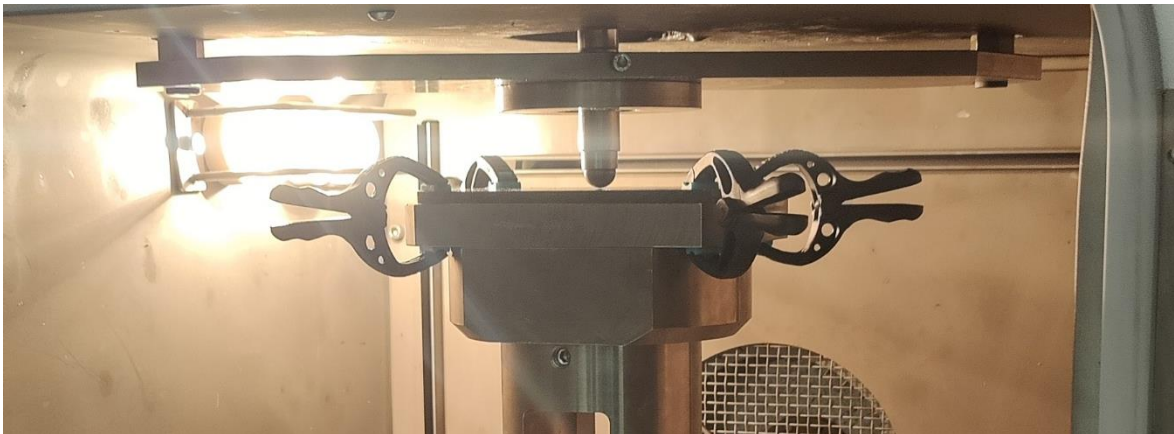

Figure 8: Drop weight impact testing machine with specimen on place

Throughout the testing procedure, the drop height was maintained at 200 mm, and the velocity remained constant at 1.98 m/s. The specimens were positioned within an impact support fixture and secured at their four corners using identical clamps, as depicted in Figure 8. The force experienced over the loading time was recorded by a load cell situated on the drop bolt. Using this recorded data, the operating software of the apparatus computed the force-time curve and derived impact energies. The ASTM D7136 standard permits adjustments to the applied impact energies by adding or subtracting corresponding supplementary weights.

For this study, a uniform impact energy of 20 J was chosen for all specimens. This decision was informed by prior testing conducted within this research. A more extensive discussion of this choice is presented in section 5.2.

4.7 Compression after impact setup

Compression After Impact (CAI) tests are conducted according to ASTM D7137 standard [32]. These tests are conducted utilizing the universal tensile-compression testing machine, model 5500R, from Instron GmbH located in Darmstadt, Germany. The testing apparatus is equipped with a 100 kN load cell, as illustrated in Figure 9. In the testing procedure, the specimen is positioned on an open chamber with dimensions of 100 mm x 150 mm. It is securely held and fixed from all four sides within this chamber.
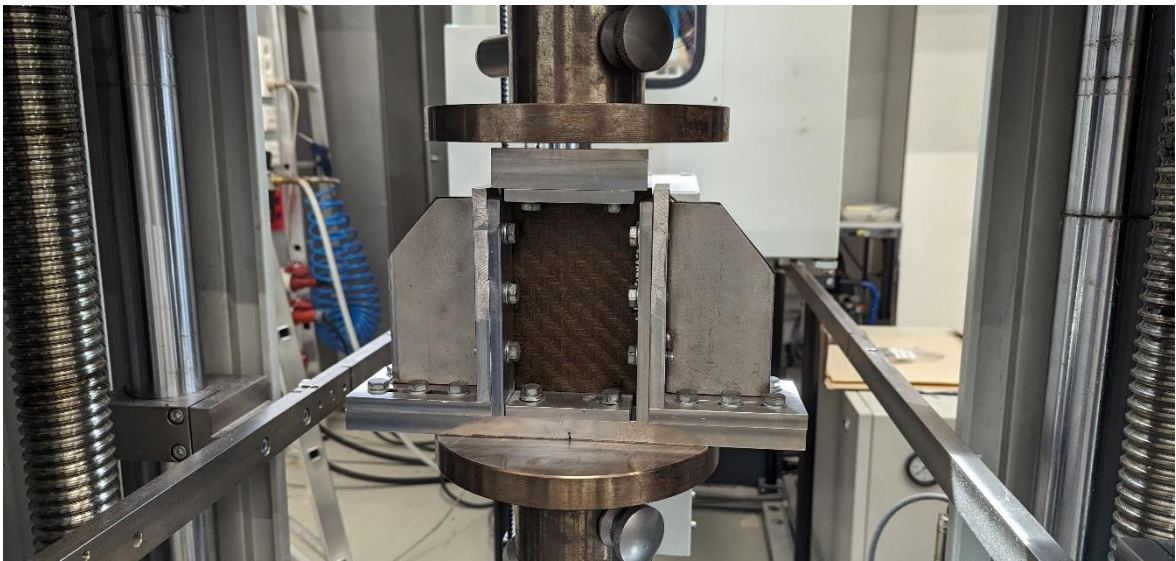
Figure 9: Compression after impact testing setup

The test operates with the upper flexible part of the equipment moving at a vertical speed of 0.5 mm/min. In the case of epoxy-based specimens, the test is halted upon fracture. However, for vitrimer-based specimens, a different approach is taken. The test for these specimens is set to continue until a maximum displacement of 4.0 mm is reached after achieving ultimate strength. This approach is chosen due to the composite's plastic behavior, allowing it to deform without necessarily reaching a point of fracture.

4.8 Injection repair setup

Two distinct repair methodology for injection repair of epoxy-based specimens were evaluated in this study. Here, a concise overview of both approaches will be provided. Additionally, in section 5.4, specific outcomes will be detailed to substantiate the chosen repair strategy.

4.8.1 Vent hole approach

It has been suggested in the literature that the delamination of plies of existing composites in aeronautic applications may be repaired using injection [8, 9, 12]. A pivotal preparatory step for this process involves drilling holes into the affected composite. Specifically, two types of holes are introduced: a resin injection hole (RH) positioned within the impaired region, and a sequence of vent holes (VH) located at the periphery of the affected area. This configuration is illustrated on the left side of Figure 10. The vent holes serve a dual purpose: firstly, they expel displaced air from the damaged and cracked area, and secondly, they create a passage through which the resin can flow out of the impact zone, as depicted on left lower left side of Figure 10. On the right side of Figure 10, visual representations of the 150 mm x 100 mm impacted specimen are showcased, offering different perspectives on the configuration.
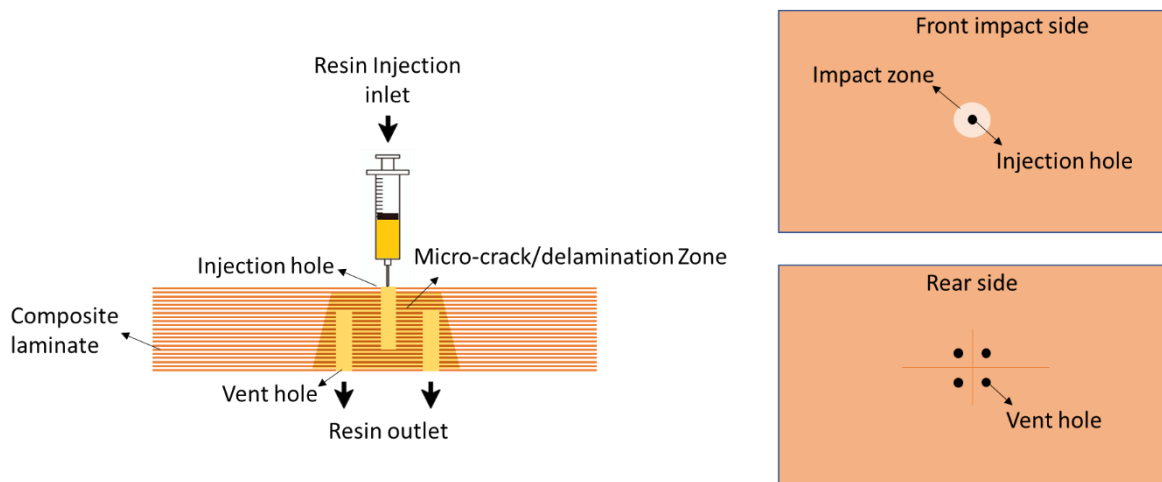

Figure 10: Resin infiltration on damaged specimen with four vent holes

4.8.2 Vent hole-less approach

Based on findings related to potential harm caused by drilling flax-reinforced composites as reported in prior studies [10, 11], a concern arose regarding the possibility of further damage incurred during the drilling process of the specimens. Furthermore, initial results from the NDT IR thermography showed artifacts caused by vent holes that remained unfilled by the resin which could potentially compromise the accuracy of the already successful measurements. Consequently, these observations prompted a reevaluation of the approach, leading to the consideration of a vent hole-less alternative, as documented in the existing literature [9]. The vent hole-less method, depicted in the left side of Figure 11, emerged as a more effective and less intrusive alternative. In this approach, a resin injection hole is introduced into the specimen. Preliminary experimentation with this technique revealed that despite the absence of vent holes, the dual functionality of vent holes — displacing air and accommodating injected resin — can be substituted by employing a vacuum from the rear side of the specimen. This configuration is demonstrated on the right side of Figure 11.

The presence of microcrack network and delamination within the damaged specimens will create pathways for the resin to flow through as depicted on left lower left side of Figure 11. Simultaneously, the vacuum operation facilitates the displacement of air out of this micro-crack network [9, 12].
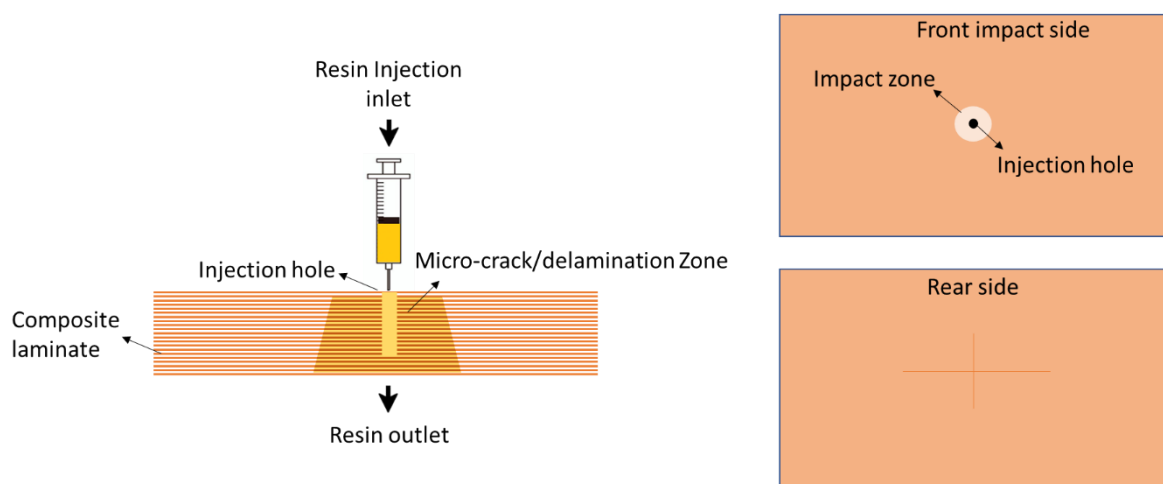

Figure 11: Resin infiltration on damaged specimen with no vent holes

Among the available approaches, this method was deemed the most suitable for repairing the epoxy-based specimens that had been impacted. To execute the drilling process, a High-Speed Steel (HSS) twist drill bit with a diameter of 2 mm was employed. The drilling was performed using a press table drill, specifically the FM 45 HS Bernardo PWA HandelsgesmbH (Linz, Austria), as depicted in Figure 12a and 12b. The drill's rotational speed was set to 2000 rpm, as shown in Figure 12a, and a feed rate of 0.02 – 0.06 mm/rev was employed. The drilling depth was established at 75 % - 80 % of the total width of the specimen, as illustrated in Figure 12c.
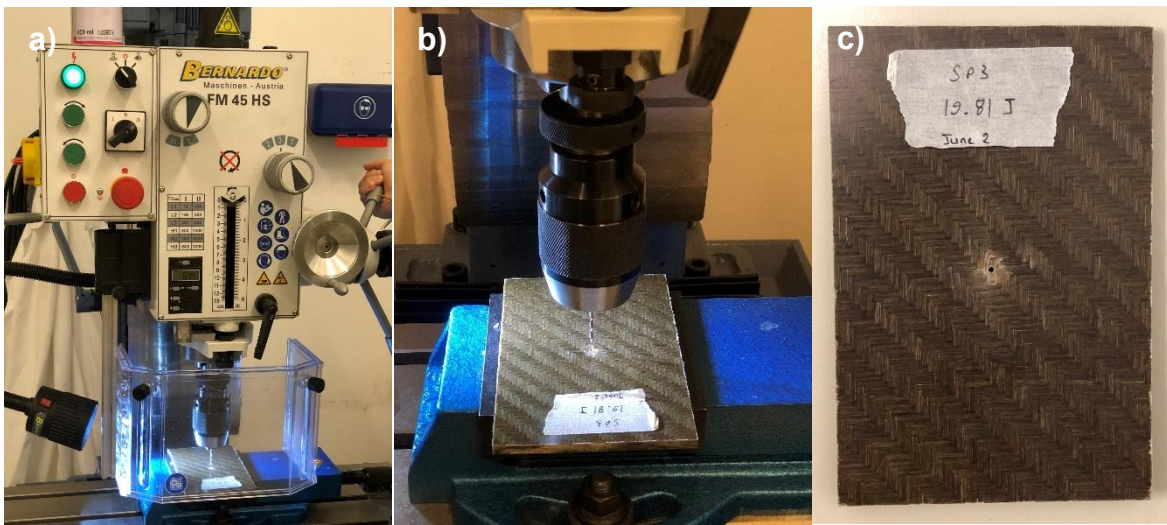

Figure 12: Setup of epoxy-based specimens drilling
a) Drill set at 2000 rpm. b) Drilling close-up. c) Close-up of drilled specimen

Figure 13 provides a visual representation of this selected approach. In this depiction, the impacted specimen is wrapped by both a release peel ply and a breather cloth. This arrangement functions as a channel, allowing displaced air and resin to flow uniformly from the rear side of the specimen [12]. To establish a controlled environment, a vacuum bag is carefully placed around this setup. Sealant tape is employed to ensure that the resin is introduced solely through the designated injection hole. Inlet and outlet tubes, along with valves, are positioned appropriately. The vacuum system is then activated. During this phase, any air leaks that are detected are identified and resolved through adjustments to the sealant tape as needed.
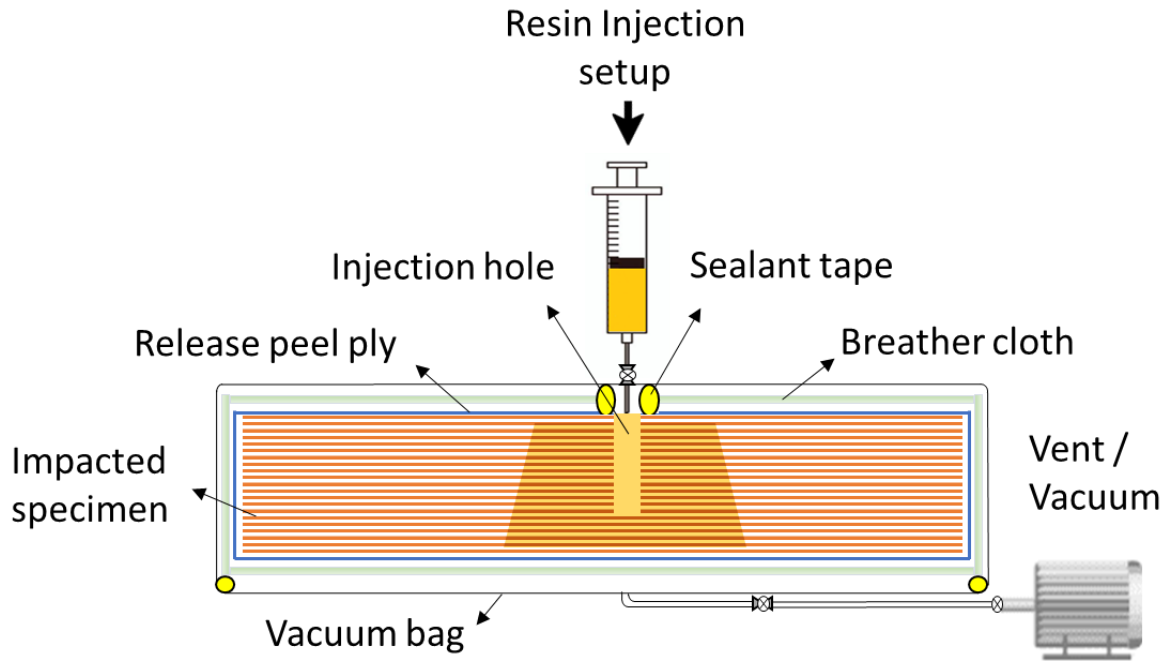
Figure 13: Schematic of epoxy-based specimens repair setup

The injected resin was formulated using the same resin-to-hardener by weight ratio as the infusion resin (100:25). This mixture was prepared in a slightly reduced quantity, sufficient to fill a 20 ml syringe. The syringe was positioned atop the damaged specimen throughout both the injection phase and the subsequent curing process.

Once the vacuum system was activated and any air leaks were appropriately addressed, the injection process was initiated by simultaneously opening the inlet and outlet valves. Promptly, the resin began to flow into the interior of the damaged specimen, facilitated by the vacuum's displacement of air. Moreover, to ensure the effective injection of resin into the damaged area, a pressure of ~1-2 bar was maintained from the syringe throughout the process. This measure ensure the success of the resin injection process within the damaged specimen.

Following a duration of 10 — 15 minutes, the injection procedure was stopped by closing the inlet and outlet valves, as depicted in Figure 14. Subsequently, the syringe was carefully removed, and the outlet tube was detached. The complete assembly, as displayed in Figure 15a and 15b, was transferred to an oven set at 80 °C, where it was left to cure for a duration of 1 hour.

Figure 14: Injection repair process.
a) After 1 minute. b) After 5 minutes. c) After 10 minutes

Upon the completion of the curing phase, the consumables — namely, the vacuum bag, release peel ply, and breather cloth — were carefully removed from the repaired specimen. The resin infusion effectively filled the voids created by the drilling process. Furthermore, any residual traces of the sealant tape were carefully removed from the surface of the repaired specimen.
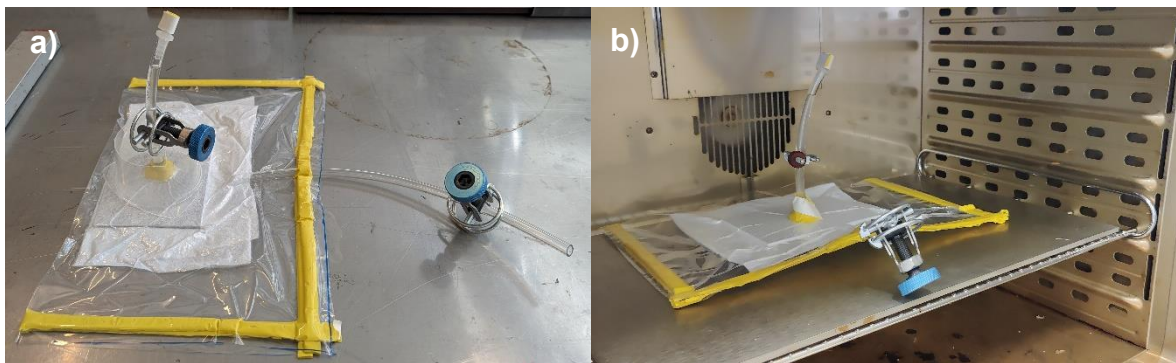

Figure 15: Setup of epoxy-based specimens repair approach
a) Repair setup after injection prior to curing in the oven. b) Injection setup inside the oven set at 80 °C

4.9 Forming setup

To facilitate the restoration of damaged specimens made from vitrimer material, the resin needs to undergo a forming process, allowing it to attain the vitrimer transition temperature (Tv). In the case of the specific resin chosen i.e. ELSO + GA +TBD, the anticipated vitrimer transition temperature is 160 °C, as indicated in reference [23]. It has been noted that maintaining the resin above its Tg for a minimum of 3 hours is necessary to relax internal stresses within the material and promote vitrimeric characteristics.

The methodology employed in this study follows the configuration depicted in Figure 16. The impacted specimen is positioned upon a movable press and pre-heated to

a temperature of 160 °C. To prevent the specimen from sticking to the press's surface, Kapton® Polyimide film is situated both above and below the specimen.
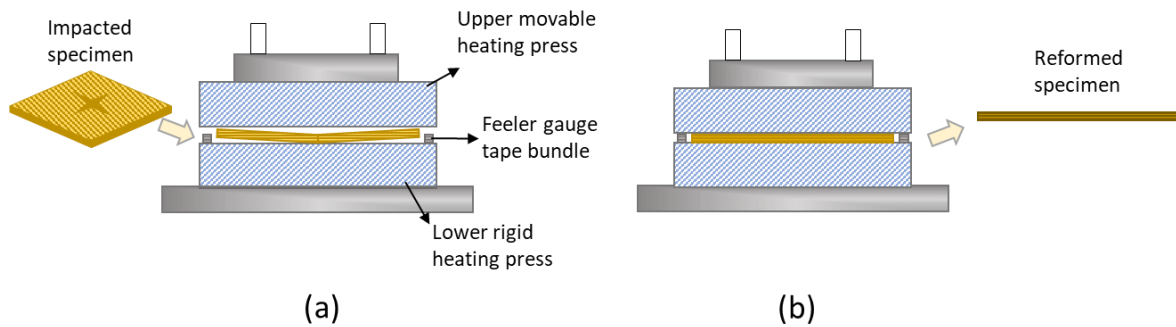

Figure 16: Schematic of vitrimer-based specimens repair setup
a) Impacted specimen is placed on press at 160 °C. b) After four hours the specimen is reformed

Prior to initiating the repair process, the thickness of each specimen is measured. Subsequently, a bundle of feeler gauge tape with the original thickness of the specimen is placed alongside the specimen, as depicted in Figure 17a. This strategic placement serves to establish the minimum thickness of the flexible specimen, effectively maintaining its initial dimensions. This precaution prevents excessive compression during the press operation, a condition that could potentially lead to ply displacement, misalignment, and buckling within the composite structure. By maintaining the specimen's original thickness, the structural integrity of the material is preserved during the heating and repair process.

After achieving a temperature of 160 °C on both sides of the press, the polyimide film, specimen, and bundles of feeler gauge tape are carefully arranged, as depicted in Figure 17b. Subsequently, the press is gradually lowered until it contacts both sides of the specimen. Then the press was gently brought down in a controlled manner for a duration of 10 minutes in order to restore the specimen's shape which was deformed due to the impact, as depicted if Figure 16.

As the press reaches the point where the feeler tape bundles create a natural stopping point on both sides, a consistent compressive load of approximately 4 - 8 kN is sustained. This load is maintained throughout the entirety of the reforming process, which spans a duration of 4 hours for each individual specimen, as shown

in Figure 16b. After this 4-hour interval has transpired, the press is carefully disengaged, and the specimen is subsequently extracted.
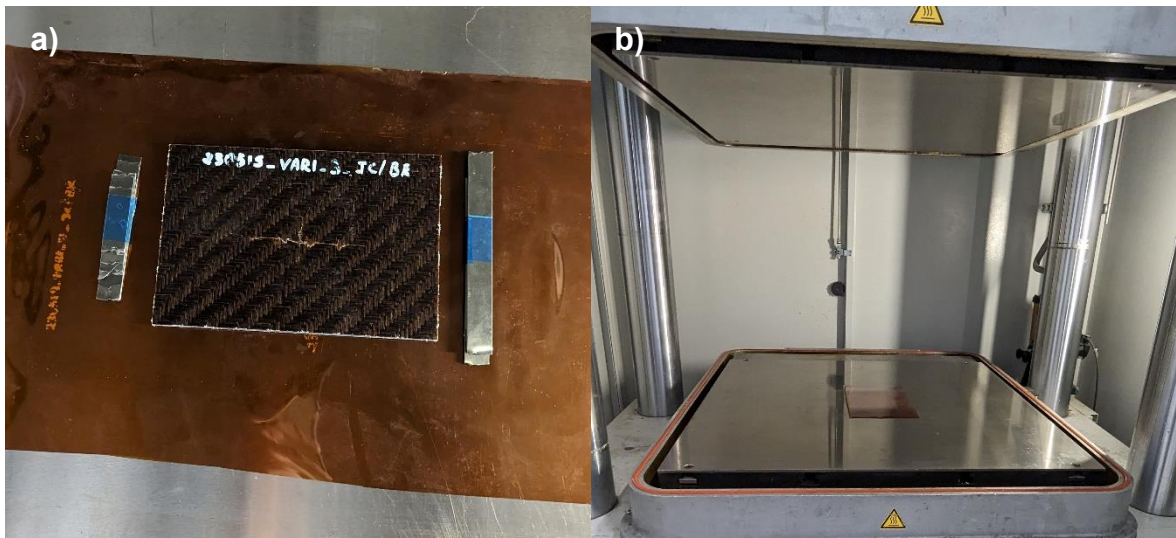

Figure 17: Setup of vitrimer-based specimens repair approach
a) Damaged specimen on place between gauge tape bundles. b) View of the heating press prior repairing

A notable outcome of this reforming process at an elevated temperature is the alteration in the specimen's color. This change is potentially attributed to the thermal degradation that might have affected both the fiber and matrix constituents. A comprehensive exploration of this phenomenon is offered in section 5.8.2.

5 Results and discussion

5.1 Flax vitrimeric-based composite manufacturing trials

To produce the NF-Vi plate described earlier, a series of processing techniques were explored initially to achieve a compact and balanced composite structure. One effective strategy involves enhancing the resin impregnation between the fibers. This improvement in impregnation has been correlated with a slight reduction in fiber content in vitrimer-based composites [33]. Fiber content quantification can be achieved by assessing the mass of raw materials prior to composite plate fabrication. The calculation of fiber mass ratio psi_f is accomplished using Equation 1, where the total mass of the demolded composite m_C is compared against the mass of dry fibers m_{DF} before resin infusion.

$$psi_f = \frac{m_{DF}}{m_C}$$
1

The viscosity of the vitrimer-based resin played a critical role in the infusion process, thereby necessitating constant temperature monitoring and control throughout all stages of VARI. To assess the resin's infusion behavior, a series of tests were conducted to identify the optimal conditions. These tests utilized 5 layers of the aforementioned flax fiber, each layer measuring 250 mm x 250 mm. The specific conditions for each trial are documented in Table 2. The remaining conditions were kept consistent with those outlined in section 4.3.2.

Trial #1 revealed that, despite elevating the resin's temperature using a magnetic stirring heating plate, the viscosity was still too high to facilitate the desired flow within the flax fibers within the intended infusion timeframe. This optimal infusion time ranged between 8 and 15 minutes for the size of the composite plate being used. After a total infusion time of 25 minutes in this trial, it became evident that the resin was unable to flow effectively within the flax due to its high viscosity.

In response, Trial #2 was executed by introducing a flow media atop the release peel ply. This alteration resulted in a noticeably lower infusion time of 5 minutes. However, this approach led to an uneven flow front, where the central region advanced too swiftly compared to the sides. This disparity in flow rates resulted in

an inconsistent flow pattern across the entire plate. Notably, this trial also served as a platform to evaluate the resin preparation process. It was discovered that preparing the resin proved to be a somewhat laborious task, with glutaric anhydride in crystal form taking 26 minutes to fully disperse and homogenize within the resin.

Table 2: NF-Vi trial plates

	T1	T2	T3	T4
Heating media	Heating plate	Heating plate	Oven	Oven
Flow media layer	No	Yes	Yes	No
Anhydride form	Powder	Powder	Melted	Melted
Mixing time (Min)	30	26	5	5
Infusion time (Min)	25	5	10	23
m_{DF} (g)	190.01	172.85	167.35	101.49
m_C (g)	377.19	405.57	444.46	222.43
psi_f	0.50	0.43	0.38	0.46

Equipped with the insights gathered, trial #3 was executed following a methodology similar to trial #2. However, a modification was introduced in the resin preparation process. In this instance, both the resin and hardener were placed within an oven at a temperature of 80 °C during 45 minutes. This elevated temperature caused the glutaric anhydride to melt, facilitating a thorough mixing process accomplished within 5 minutes. This was succeeded by a 1-minute degassing phase. Notably, a previous degassing stage was conducted while combining the ELSO and TBD components. With this alteration, the infusion process was successfully completed within a 10-minute timeframe. The reduced fiber mass content observed in trial #3

was attributed to enhanced fiber impregnation and interlaminar presence, contrasting with trial #2, where the flow front was less uniform.

Trial #4 aimed to reproduce the approach of melting the glutaric anhydride while assessing the reproducibility of achieving improved mixing time with comparable results. In this instance, the flow media layer was not employed as the goal of the experiment was to determine whether the more uniform heating achieved in the oven and the reduced mixing duration would yield a resin with lower viscosity and higher temperature, potentially resulting in a reduction in infusion time. However, trial #4's infusion period stretched to 23 minutes, thus confirming that, for the selected vitrimeric system operating temperature, the incorporation of a flow media layer remains essential.
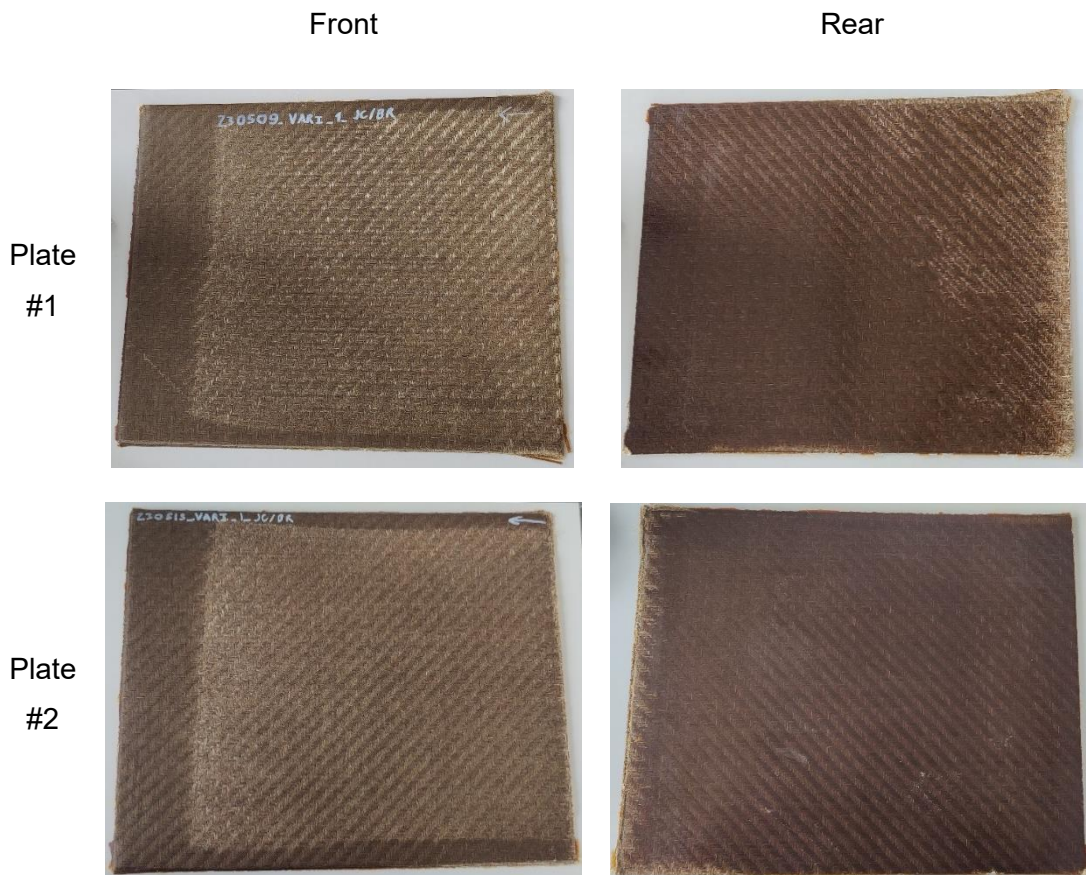

Figure 18: Front and rear side of NF-Vi plates (550 mm x 350 mm)

The approach utilized in trial #3 aligned with section 4.3.2. This method was also adopted for fabricating the plates of dimensions 550 mm x 350 mm as seen on

Figure 18, that were subsequently utilized in the creation of the vitrimer specimens. Both of these NF-Vi plates exhibited a consistent fiber mass ratio of 0.42. However, their infusion times varied, standing at 21 minutes and 16 minutes, respectively. The principal distinction between these plates was their thickness, culminating in an average thickness of 5.30 mm and 5.41 mm, respectively.

5.2 Drop weight impact energy trials

Previous to inducing damage on the chosen specimens, a predefined damage level needed to be established consistently across all samples. Initially, two scenarios were considered: one involving solely matrix damage while the fibers remained intact, and the other entailing damage to both the matrix and fibers.

To determine the optimal energy level for inducing damage, a range of impact energies was contemplated and subsequently tested for both the epoxy-based and vitrimer-based specimens. Specifically, impact energies of 10 J, 15 J, 16 J, 17 J, 20 J, 25 J, and 30 J were evaluated. The process commenced by impacting all the epoxy-based specimens, targeting their reflective surfaces. This procedure was then followed by a continuation with the vitrimer-based specimens.

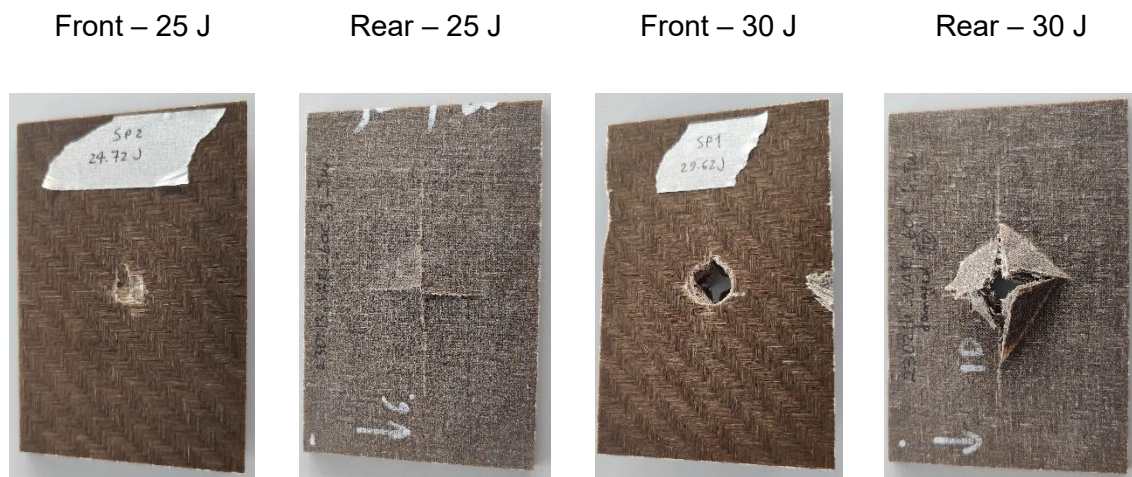Front – 25 J   Rear – 25 J   Front – 30 J   Rear – 30 J

Figure 19: Impact tests of 25J and 30 J for epoxy-based specimens

As testing progressed, it became evident that any impact energy exceeding 20 J had to be discarded due to the extent of the inflicted damage. This conclusion is illustrated by Figure 19, which showcases instances of severe damage and even complete puncture of the composite's in the case of the 30 J impact energy.

Consequently, only impact energies ranging from 10 J to 20 J were applied to the vitrimer-based specimens. This discerning approach was driven by the intent to maintain controlled damage conditions and ensure the structural integrity of the specimens during testing.

To determine the most suitable impact energy for the specimens, flash thermography was employed to demonstrate the presence of non-visible delamination within the composite specimen as illustrated in Figure 7.

Thermography images are captured at a frequency of 5 Hz over a 100-second duration. The choice of this 100-second interval stems from the fact that it is the average time the composite plate takes to reach and sustain a stable temperature for a period of time before the temperature drops. Figure 20 provides an example using the 20 J epoxy-based damaged specimens as the subject of examination.
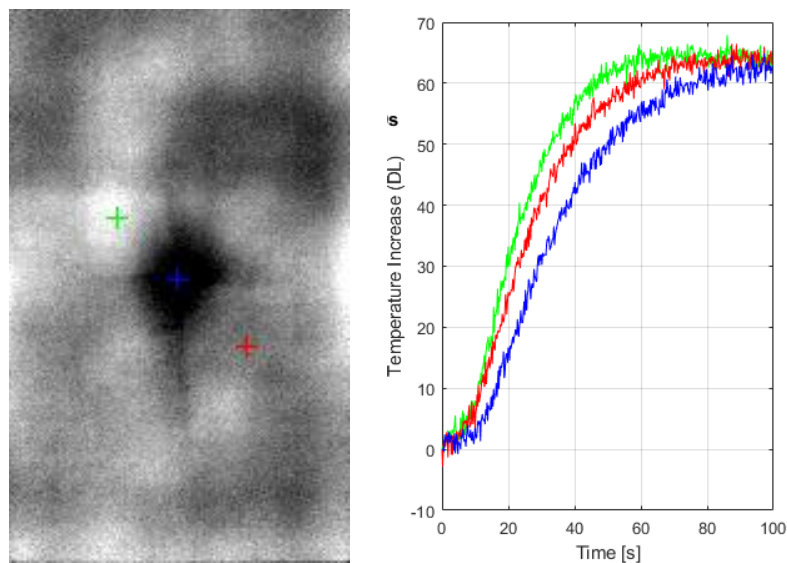

Figure 20: Thermography of impacted epoxy-specimen 20 J– Temperature profile difference

In this context, the darker regions within the image indicate areas where the temperature has increased in a slower rate. The clearer, whiter sections denote the converse — areas where temperature elevation has occurred at a faster pace. This contrast is evident in the right side of Figure 20, where the undamaged green spot showcases a more rapid temperature increase compared to the damaged blue spot. Notably, the thermal insulation evident in the darker portions may result from matrix

damage. This observation aligns with the scenario illustrated in Figure 20, marked in blue. The diminished thermal conductivity associated with fragmented matrix systems — causing pockets of air between fractured matrix-matrix systems and between matrix and fiber — contributes to this outcome.

Given the intricate composition of composites involving non-uniform layers and the variable compaction pressure profiles resulting from the VARI process [34], it is expected that the thickness variation will lead to distinct local composite compositions. These compositions are likely to manifest as an intensity profile in the thermographs.

Also, darker regions that appear widely spread beyond the impacted zone during thermography analysis of composite specimens could also be indicative of several underlying factors such as residual stress, uneven thermal contact, surface finish variations, or thermal inertia. During impact events can introduce residual stresses in the material, which may result in localized temperature variations due to differences in thermal conductivity and heat dissipation. These residual stresses can cause heat accumulation or redistribution, leading to temperature variations that show up as darker spots in thermographic images. Furthermore, uneven thermal contact between the specimen and the thermographic equipment or variations in surface finish or texture can affect the emissivity of the material, which impacts its ability to emit infrared radiation. Differences in emissivity can lead to variations in measured temperatures and consequently result in darker spots. Certainly, this explains potential factors that can lead to discoloration or darker regions in the thermographs that are illustrated in the present work.

In Figure 21 and Figure 22, we can observe the post-impact visual representation of the epoxy-based and vitrimer-based composites respectively. The sequence includes images of the front side, followed by the rear side, and thermography pictures. Notably, in Figure 22, for the 10 J impact case, even though there is no visible impact damage on the front side (highlighted in red) and no apparent dent, a slightly darker irregular spot can be observed in the thermographs around the impact point at the center. This suggests a combined failure of both the fiber and matrix.

This conclusion is supported by the rear side view of the specimen, confirming such damage.

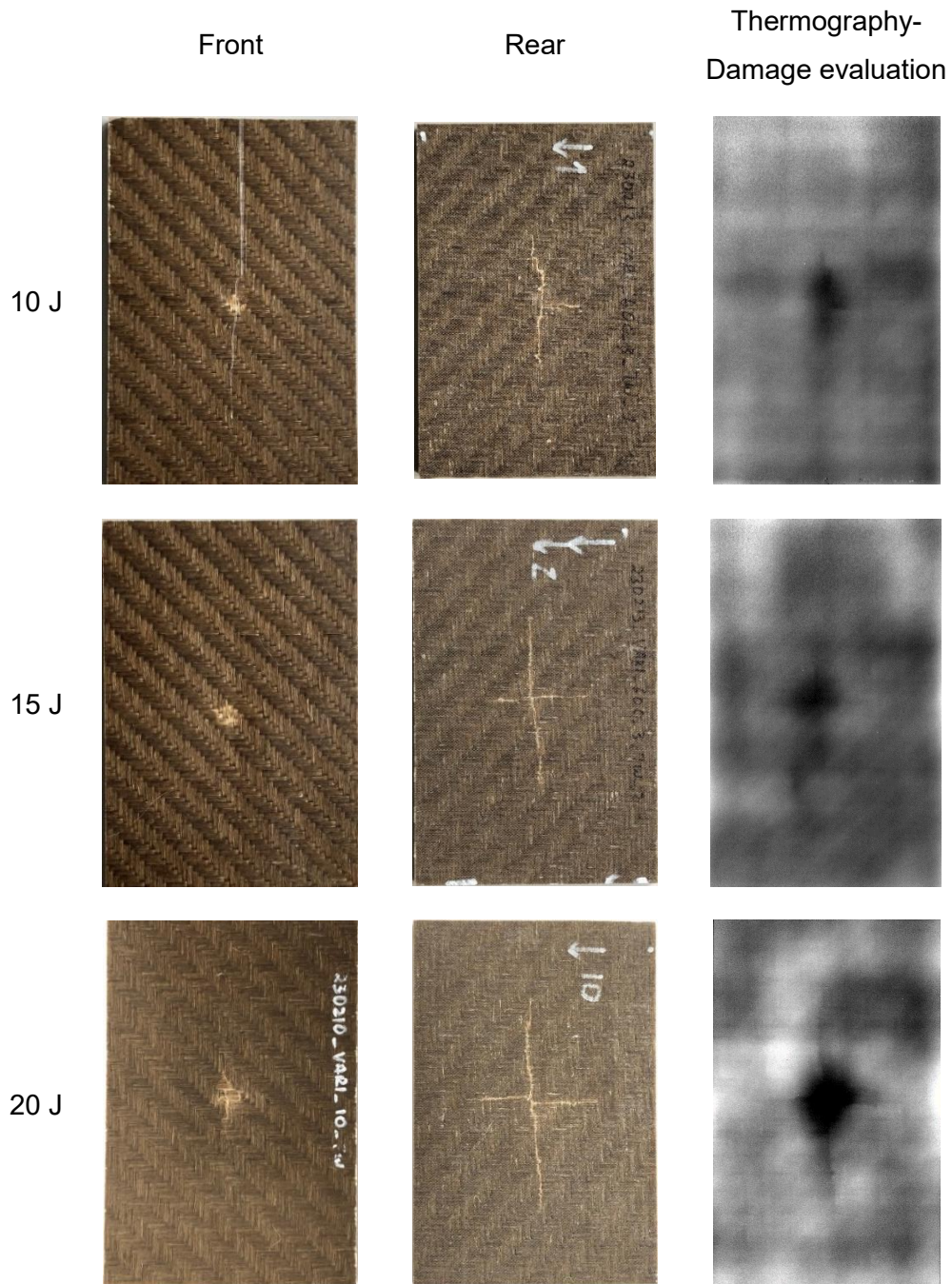|	Front	Rear	Thermography- Damage evaluation
10 J			
15 J			
20 J			

Figure 21: Front, rear and thermography image of impacted epoxy-based specimens

An evident conclusion drawn from the analysis of Figure 21 and Figure 22 is that higher energy impacts result in visible damage on the front side of the specimens. Thermography analysis explicitly reveals the presence of a predominant cross-

shaped crack caused by fiber breakage on the rear side, indicating internal damage. These findings underline the significance of employing both visual inspection and thermography techniques to comprehensively understand the damage evolution in composite materials.
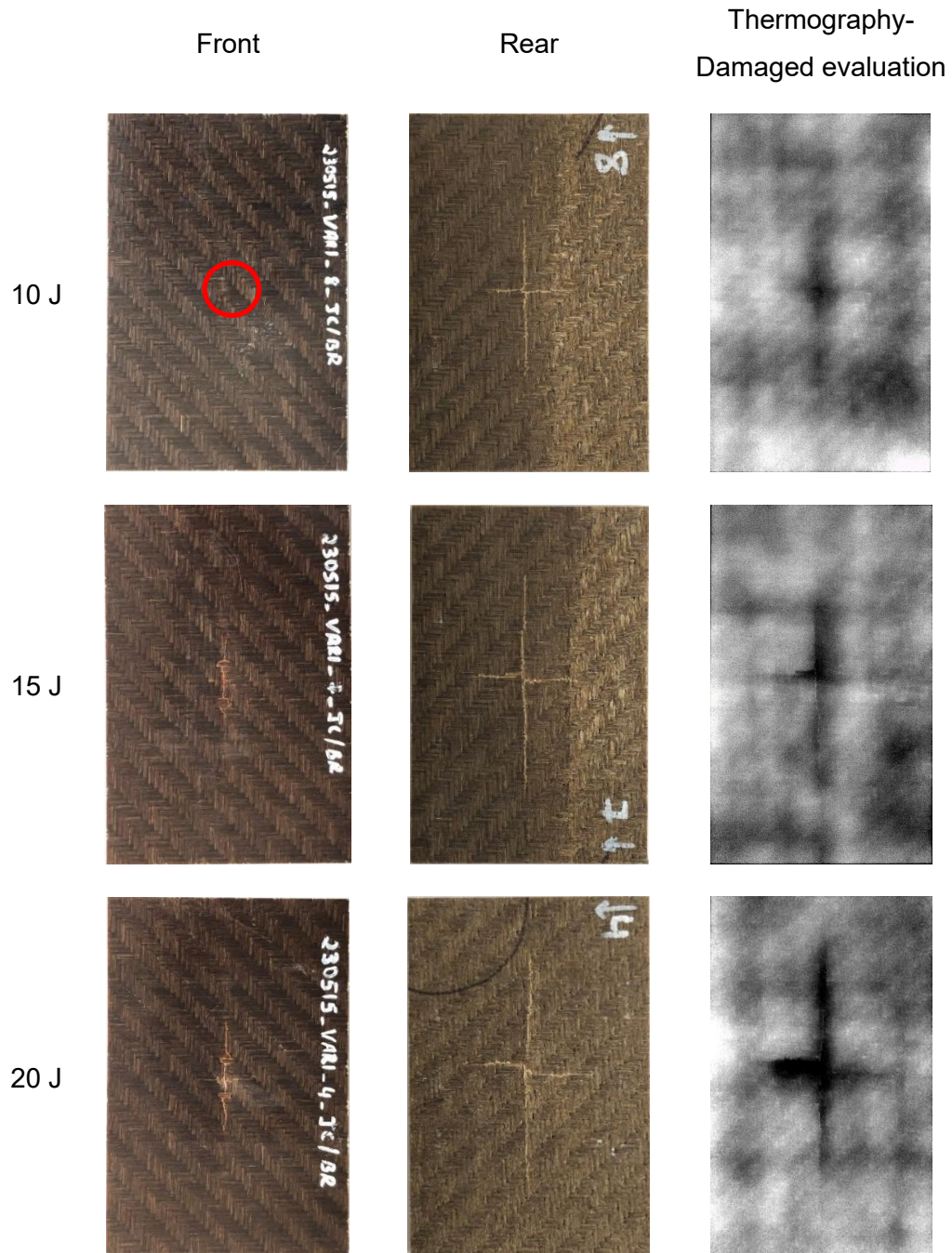

Figure 22: Front, rear and thermography image of impacted vitrimer-based specimens

Following a thorough assessment of these outcomes, the decision was made to subject all selected specimens to a uniform damage level. The impact energy of 20 J was chosen for this purpose. This energy displayed both fiber breakage and matrix damage without causing excessive perforation through any layer of the composite, as seen with the 25 J impact. Moreover, substantial matrix damage is necessary to establish a network of micro cracks and internal delamination within the NF-EP, a crucial aspect correlated with the effectiveness of the chosen repair approach [35], as depicted earlier in Figure 11.

5.3 Drop weight impact quantitative results

The sensor instrumentation of the drop tower facilitates the measurement of several impact-related parameters, such as contact force, duration, and displacement records of the impactor. Figure 23 presents three distinctive graphs that can be derived from this dataset. Initially, in Figure 23a, the Load vs Time plot illustrate the contact time, with the load and unload phases caused by the impact. The loading phase's non-linear behavior signifies the internal damage inflicted upon the composite, progressing until it reaches the maximum load, referred to as the "peak force" of the material. Subsequently, the unloading phase takes place. During impact, the graph displays oscillations characteristic of vibrations triggered by the impact [36]. In Figure 24a, the same plot is depicted for two of the selected specimens that were subsequently repaired. Importantly, in the case of the NF-Vi, a longer contact time is evident in the graph, indicating a more prolonged interaction during impact compared to other cases.
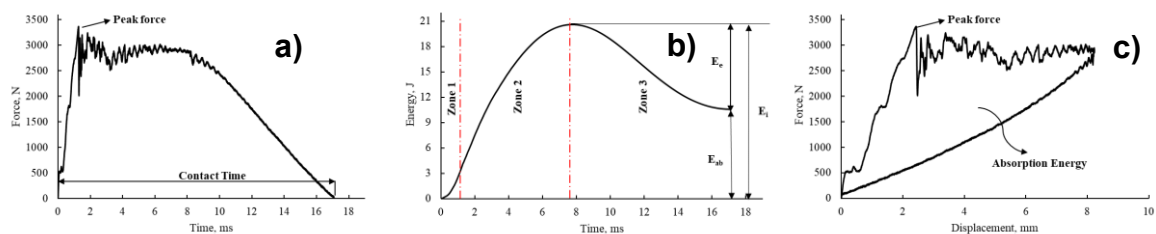

Figure 23: Example of typical characteristic plots of impact with key details highlighted

The Energy-Time curve, Figure 23b, unveils key aspects of the impact. To begin, the Zone 1 delimited area illustrates the initial slope of impact, culminating in Zone 2, which represents the point of maximum impact energy transfer to the specimen.

In zone 3, after reaching the peak impact not all of the kinetic energy is released, signifying that the energy was directly absorbed by the specimen [37]. Throughout the impact, the absorbed energy is divided between elastic deformation and plastic damage. The energy curve initially ascends until it reaches the impact energy, then descends before stabilizing. The energy value at the test's conclusion corresponds to the permanent deformation induced by various damage mechanisms. As evident in Figure 24b, an impact energy of 20 J led the vitrimer-based specimen to absorb more energy than its epoxy-based counterpart.
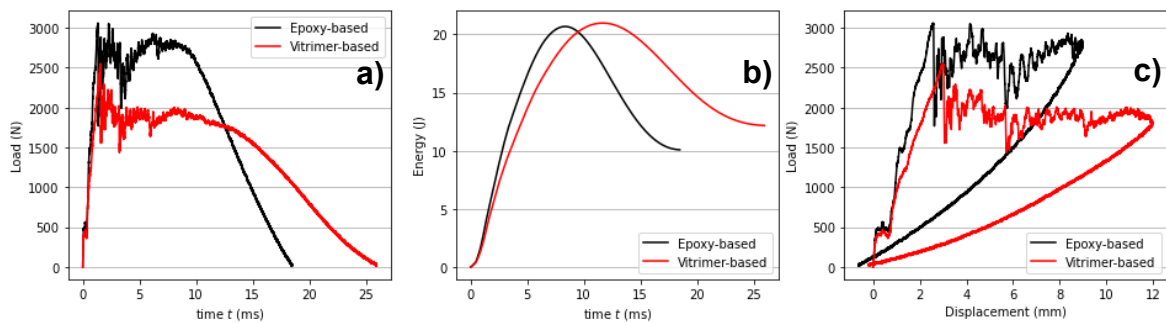

Figure 24: Characteristic impact plots for average impacted specimens

Figure 23c represents the Load vs. Displacement plot. The displacement values in this graph denote the deformation of the impacted surface and the motion of the impactor [38]. A higher peak force signifies a stiffer interaction between the impactor and the specimen, resulting in a shorter impactor contact period on the surface [39]. In most instances, the peak deformation coincides closely with the peak force point. However, it's important to note that the peak deformation signifies the point where the force curve returns to zero following the loading phase or ascending curve, whereas the peak force represents the maximum vertical value on the graph. Both peak force and peak deformation values are derived from distinct points [40].

In Figure 24c, comparing the results of the epoxy-based and vitrimer-based impacted specimens, it's evident that the interaction was shorter for the epoxy-based ones at a 20 J impact energy. This finding confirms the stiffer interaction of the epoxy-based specimen and clearly demonstrates that the vitrimer-based specimen absorbed more energy than its epoxy-based counterpart. This distinction is notably apparent due to the larger area covered by the vitrimer-based specimen.

5.4   NF-EP repair trials

The initial testing of the repair methods outlined section 4.8 involved the vent hole approach [8]. For this assessment, a 15 J impacted specimen was utilized. In Trial #1, five through holes were drilled, with one serving as the injection hole positioned at the center of the impact mark, and the other four as vent holes situated 10 mm away from the injection hole, as shown in Figure 25.
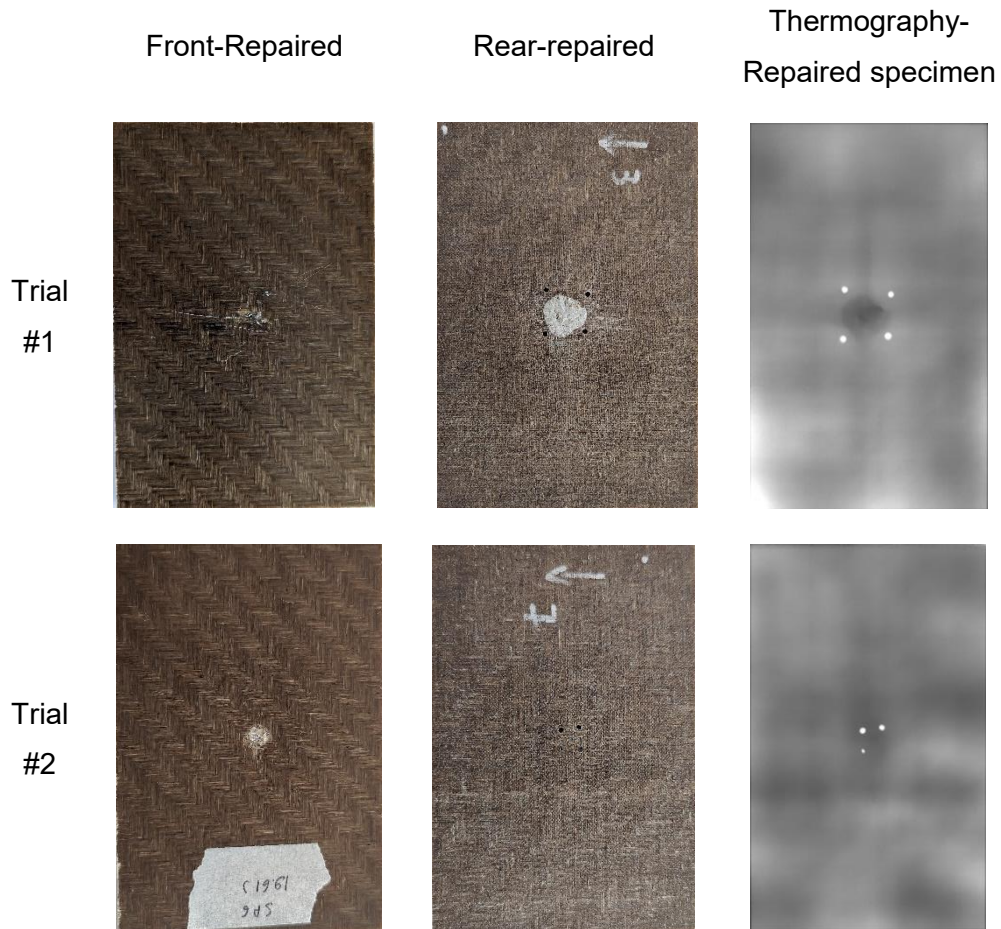

Figure 25: Front, rear and thermography image of NF-EP specimen repair trials

For the injection repair approach to be effective, it was essential to seal the injection hole, allowing resin to flow through the cracked and partially delaminated area around the impact, exiting through the vent holes [8]. To enable the injection repair approach, the injection hole needed sealing with a conventional epoxy-type sealant, with residue visible in Trial #1's rear view in Figure 25.

Subsequently, resin injection was conducted as previously described, aided by vacuum assistance to remove air from the vent holes and a syringe to maintain the pressure needed for resin flow towards the vent holes. Unfortunately, Trial #1 yielded unsuccessful results due to resin leakage around the epoxy sealant and the injection hole. Furthermore, thermography inspection revealed light coming through unfilled vent holes, causing aberrations in the obtained images, as seen in Figure 25, where vent holes appear as white circular spots. In Trial #2, modifications were implemented. The distance between the injection hole and vent holes was reduced to 5 mm. Notably, the holes were blind holes rather than through holes, as depicted in Figure 10. The blind holes' depth was set between 75 % - 80 % of the specimen's thickness, with vent holes drilled from the rear non-reflective side and the injection hole from the front side.

During Trial #2, the injection process spanned 10 minutes. The resin's coverage was extensive, as seen on the rear-repaired side of Figure 25, primarily focusing on the characteristic cross-shaped section present on the rear side-most layer of the fabric, a result of the impact. However, vent holes were not fully filled, with only one vent hole being completely filled and another partially filled, while two remained unfilled. This partial filling could attribute to the resin primarily exiting through one vent hole, creating a path of least resistance. The vent holes' diameter (2 mm) might have been too large for the resin volume, potentially causing resin to be pulled away by the vacuum. Moreover, the uneven or blocked nature of the internal delamination, gaps and cracked zone could have influenced resin injection concentration towards unblocked paths.

The thermography of trial specimen #2 also rendered optical artifacts being caused by the light coming through directly to the IR camera, as seen on Figure 25. This caused the resulting image blur and unreliable for comparisons. These issues, combined with the possibility of further addition of damage during vent hole drilling [10], favored the venthole-less repair approach.

To explore the viability of a venthole-less repair approach, a comprehensive test was conducted using a 20 J impacted specimen. This particular specimen exhibited

a distinct type of damage characterized by delamination on its rear side, differing from the typical cross-shaped mark, as depicted in Figure 26.

Thermography- Damaged specimen   Thermography- Repaired specimen   Rear - Repaired
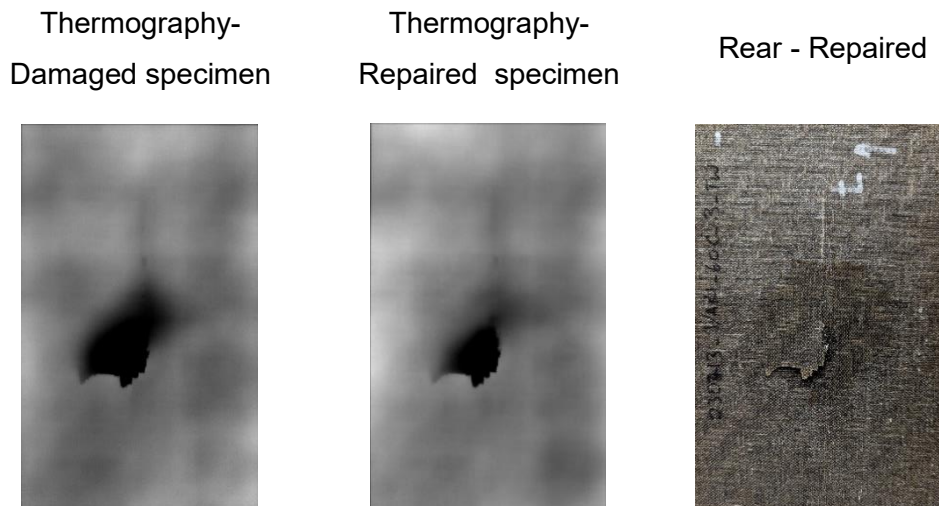

Figure 26: Thermography of third trial NF-EP specimen repair – Excessive delamination

In this experiment, only a resin injection hole was drilled, omitting the additional vent holes from the procedure. The resin infusion was carried out employing the same protocol as detailed in the previous tests. The outcome of this repair process is visually documented in Figure 26, capturing the before-and-after thermography images. Upon examination, a noticeable improvement was observed in the thermography imagery, particularly in the regions surrounding the impact zone. However, it's noteworthy that the delaminated section's condition remained largely unchanged. The gap within this delaminated area exceeded 1 mm in thickness prior to initiating the injection repair. This experimentation reveals two significant observations. Firstly, it undoubtedly confirms the practicality of the venthole-less repair approach, validating its efficacy as a viable strategy for rectifying specific types of composite damage. Secondly, it highlights a limitation of the technique in relation to extensive delamination. The absence of a rear-side compaction force throughout the injection process inhibits effective repair of substantial delamination.

5.5 NF-Vi forming trials

To explore the possibility of restoring a damaged NF-Vi specimen, an approach involving the application of pressure and temperature was investigated [22–24]. This forming approach aligned with the conditions outlined in section 4.9, necessitating the sustained exposure of the damaged composite to both continuous pressure and a temperature of at least 160 °C over a span of four hours [23].

To ensure that the applied compressive load during the forming did not exceed acceptable levels for the vitrimer composite, a bundle of feeler gauge tape was strategically placed adjacent to the damaged specimen during the reforming process. The dimensions of this tape bundle were meticulously calibrated to match or exceed the thickness of the specimen itself.

During the execution of this repair approach, it became evident that relying solely on a single bundle of feeler gauge tape was not optimal. This was apparent due to the accumulation of excessive load being concentrated on the area of the specimen positioned farthest from the tape bundle. The outcome of this load imbalance was noticeable in the reformed specimen, which exhibited ply displacement and buckling of the lower layers during the reforming process. This phenomenon is illustrated in Figure 27.

Figure 27: Ply displacement of layers in vitrimer-based specimen repair trial due to excessive load.

To address this issue, an extra bundle of feeler gauge tape was strategically positioned on both sides of the specimen, as illustrated in Figure 16. The inclusion of this supplementary bundle effectively mitigated the concentration of excessive load on the damaged specimens during the pressing process, consequently preventing further damage or modifications.

5.6 Selected repaired specimen's thermography results

To qualitatively evaluate the repair process through nondestructive means, the previously mentioned flash thermography technique was applied to three epoxy-based and three vitrimer-based specimens. These specimens underwent multiple thermography scans at various stages of the process: before damage, after damage, and after repair.

5.6.1 NF-EP results presentation

The images obtained from the NF-EP specimens exhibit a high level of clarity, as depicted in Figure 28. It's important to acknowledge that the presence of bright white spots near the specimen's edges can be attributed to an imperfect fit between the specimen holder and the specimen during the thermography procedure. This occurrence arises from the potential for light from the flash lamp to leaks around if the holder doesn't securely conform to the specimen's shape. Furthermore, in the case of selected specimens 2 and 3, it's noticeable that the damage existing prior to repair involved a minor delamination of the outermost layer. This delamination, although not extensive, was sufficiently managed by the subsequent injection repair process, leading to a satisfactory outcome.

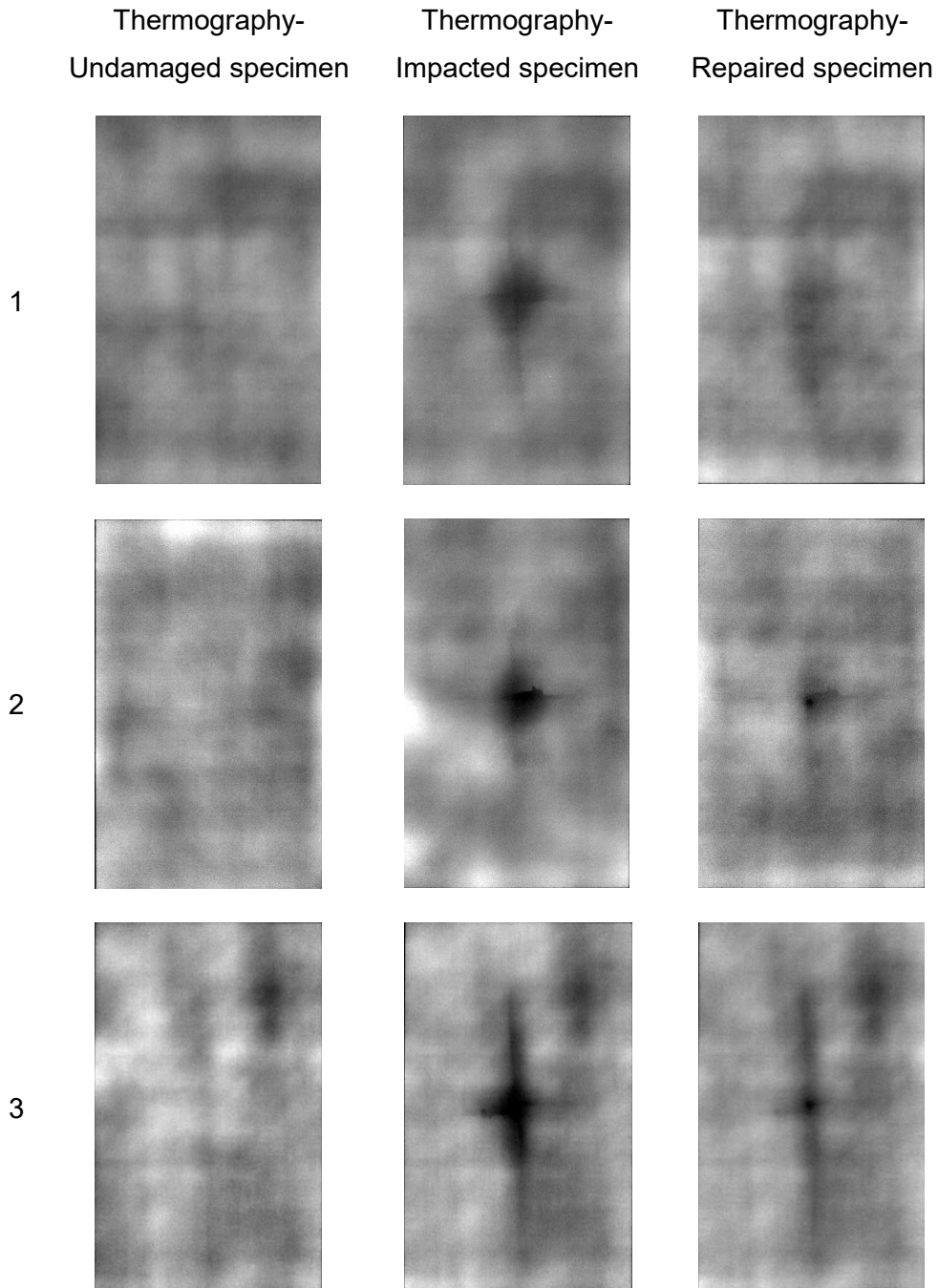| | Thermography-Undamaged specimen | Thermography-Impacted specimen | Thermography-Repaired specimen |

Figure 28 Thermographs of epoxy-based selected specimens

In Figure 29, the temperature increase graphs provide a clear distinction of the thermographed zones over time. The temperature data is normalized by referencing the highest value for a specific pixel within the 100-second time range, forming the basis of the graph construction. It's important to emphasize that the green cross, which corresponds to the injection hole, was filled with clear epoxy resin. Consequently, as the flash was triggered and the camera commenced recording,

the light and energy passed through this fiber-less region at the center of the specimen. This phenomenon resulted in a seemingly elevated initial temperature in this particular spot, as evident in both graphs. However, the temperature profile around the rest of the specimen conforms to the anticipated outcomes.
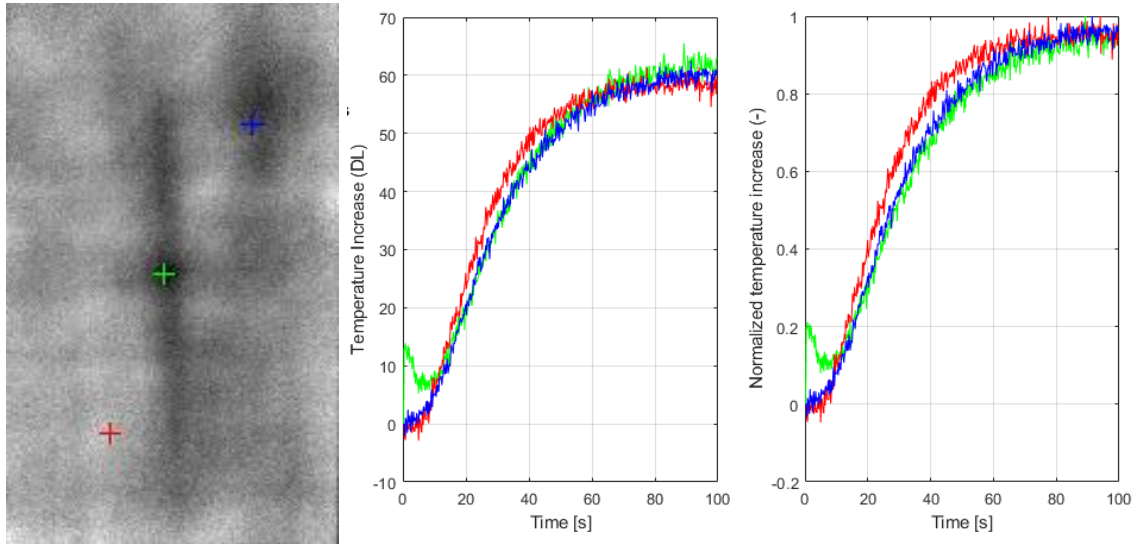

Figure 29 Thermography of repaired Epoxy-specimen #3– Temperature profile difference

Additionally, it's apparent that across all specimens, both the impact zone and its surrounding were sufficiently infiltrated with resin, leading to a more uniform appearance in the repaired thermography images. This homogeneity in the thermographic appearance indicates that the repair approach functioned as expected, successfully addressing the damaged areas.

5.6.2 NF-Vi results presentation

The thermographic outcomes of the selected three NF-Vi specimens are displayed in Figure 30. Similar to the epoxy-based specimens, the reformed vitrimer-based specimens exhibit a more uniform appearance compared to the damaged specimens. An interesting observation is that despite the slight alteration in average specimen thickness due to the reforming process, the thickness demonstrated reduced variation, as indicated in Table 6. This enhanced uniformity in thickness can be attributed to the reforming process, contributing to the overall more consistent thermographic results, evident in Figure 30.

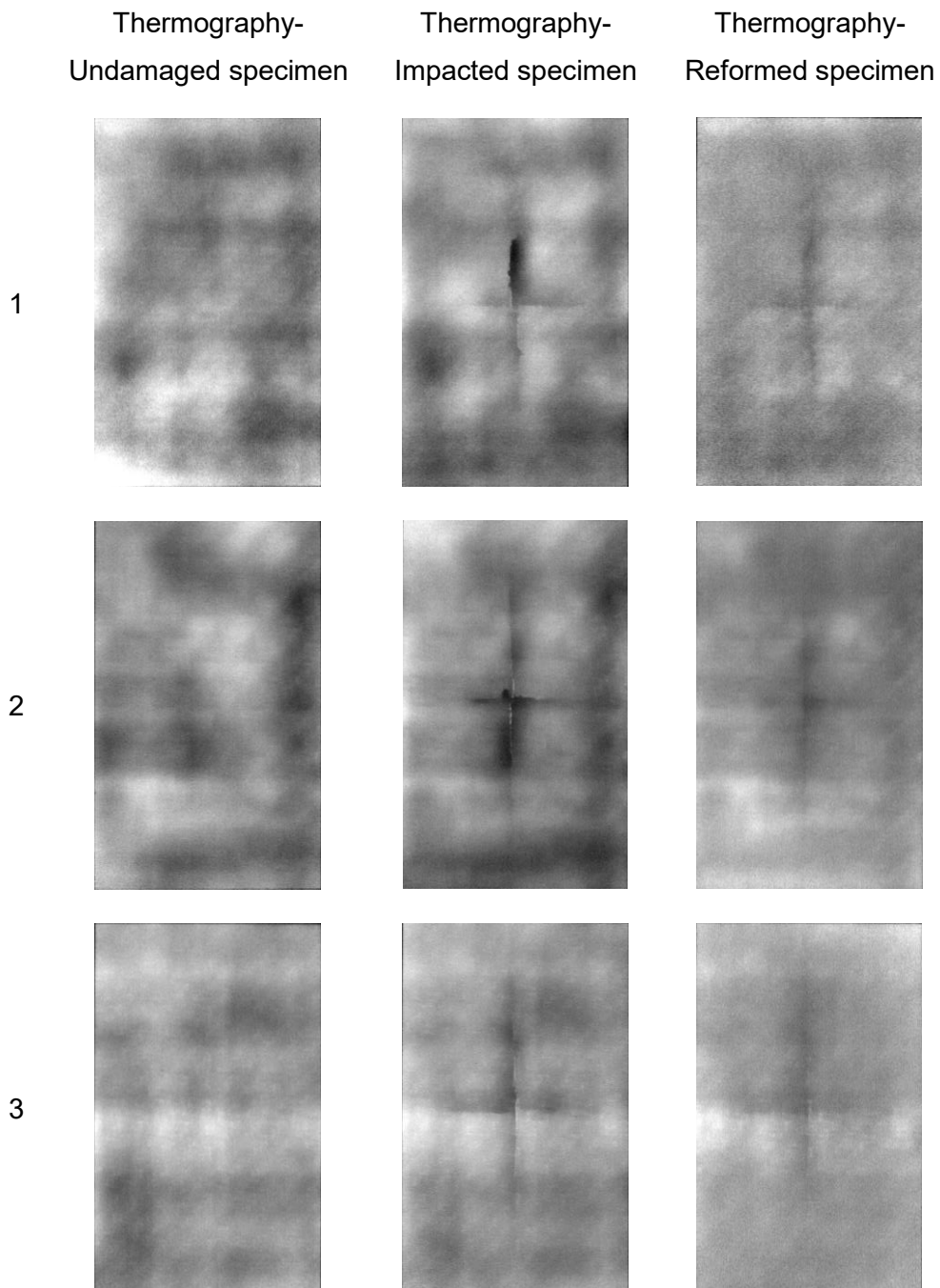|	Thermography- Undamaged specimen	Thermography- Impacted specimen	Thermography- Reformed specimen
1			
2			
3			

Figure 30: Thermographs of vitrimer-based selected specimens

It's noteworthy that the vitrimer resin's higher flexibility in comparison to the epoxy resin composite provided less impact absorption. Consequently, the fibers in the vitrimer-based specimens absorbed a portion of the kinetic energy (as discussed in section 5.3), leading to increased fiber damage compared to the other composite type. This increased fiber damage is evident in the larger and more distinct cross-section marks caused by the impact, clearly visible in the thermographs.

Qualitatively evaluating the thermographs, the reform method applied to the damaged vitrimer-based specimens appears to have been effective. Esthetic improvements were observed in the reformed vitrimer specimens, with no evident delamination and reduced thickness variation. This visual evidence suggests that the reforming method achieved its intended objectives. However, it's important to note that these visual improvements did not consistently align with the results of the compression after impact testing, which yielded contradictory outcomes.

5.7 Compression after impact results

Compression after impact was carried out for the selected repaired specimens (3), impacted specimens (3) and undamaged specimens (3) for both the epoxy-based and the vitrimer-based in a universal testing machine which measures Load vs Displacement. To present the data in compressive stress vs strain it is necessary to convert the units using Equation 2, where $\bar{B}$ means the median of the measure width, $\bar{S}$ the median of the measured thickness, and L_0 the original length of each specimen, which all corresponded to 150 mm.

To evaluate the efficacy of the repair approach and to conduct a comparative study, the specimens were subjected to compression after impact testing, comparing the results of the repaired, damaged, and undamaged specimens. For this study, a total of three specimens were selected from each of the following categories: repaired, damaged, and undamaged. These selections were made for both epoxy-based and vitrimer-based composites, resulting in a comprehensive evaluation of the different specimen conditions. This testing was conducted using a universal testing machine. To present the data in terms of compressive stress vs. strain, a conversion of units was necessary, involving the utilization of Equation 2, where F is the resulting peak load (kN) and A refers to the cross section of the composite (mm²). The standard ASTM D7137 [32] refers to the ultimate strength, which is measured in MPa. For purpose of this work, this ultimate strength will also be referred as ultimate compressive stress denoted with the symbol σ_C.

$$\sigma_C = \frac{F}{A}$$

2

The strain-stress compression behavior results are visualized in Figure 31 and Figure 33, corresponding to the epoxy-based specimens and the vitrimer-based specimens, respectively. It's important to take note of the two plates indicated in the case of the vitrimer-based specimens. This distinction arises from the constraints posed by the plate size, which can accommodate a maximum of 8 specimens. As a result, to meet the requirement specimens were sourced from two distinct vitrimer plates, as explained in section 5.1. These plates differed in terms of their thickness and weight, leading to fine variations in their mechanical properties. This variance in properties is the reason for their presentation as separate entities in the figures.
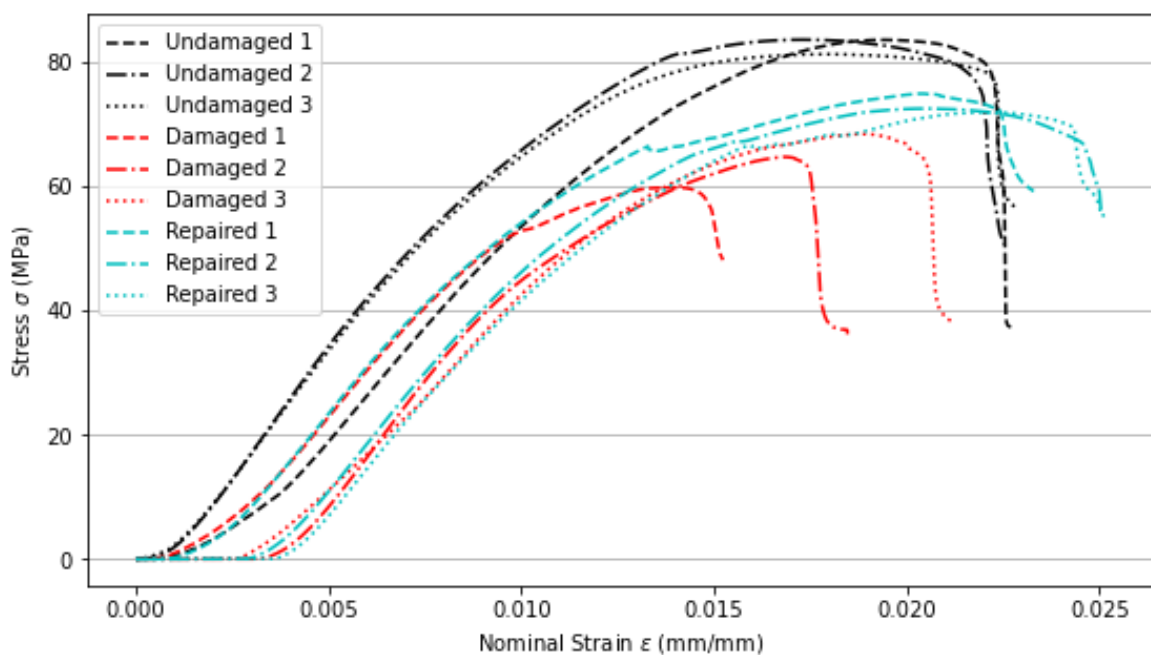
Figure 31: Representative stress-strain curve of compression after impact epoxy-based specimens

Examining the behavior of NF-EP specimens in greater detail, a clear trend emerges in the compressive strength data. The undamaged specimens showcase a notable average compressive strength, reaching approximately 82 MPa. Following closely are the repaired specimens, exhibiting a compressive strength of around 73 MPa. In contrast, the impacted specimens present a more varied response, with a compressive strength of approximately 64 MPa on average, as it can be confirmed on Table 3.

Table 3: Averaged compression loads and averaged ultimate strength for epoxy and vitrimer composites

	NF-EP			NF-Vi		
	Undamaged	Damaged	Repaired	Undamaged	Damaged	Reformed
Average load (kN)	44.835 ± 0.723	34.832 ± 2.331	39.641 ± 0.829	15.292 ± 1.411	13.577 ± 2.507	11.738 ± 2.127
Average Ultimate strength (MPa)	82.78 ± 1.34	64.31 ± 4.30	73.09 ± 1.60	28.81 ± 2.15	25.66 ± 5.11	21.92 ± 3.90

It's essential to highlight that all specimens, regardless of their category, demonstrate a consistent mode of failure characterized by lateral fracturing within the gage region [32]. This failure consistently occurs at a distance away from the middle or upper portion where the damage was initially located.

Furthermore, the failure strain for all specimens remains remarkably consistent, falling within a narrow range of 0.015 to 0.025, respectively. This pattern of fracture confirms the expected behavior and serves as a strong indicator that repaired NF-EP specimens indeed exhibit superior mechanical properties in comparison to their damaged counterparts.

In essence, these thorough observations and quantified outcomes provide compelling evidence that supports the anticipated trend, and underscores the success of the repair approach in enhancing the mechanical performance of the damaged NF-EP.
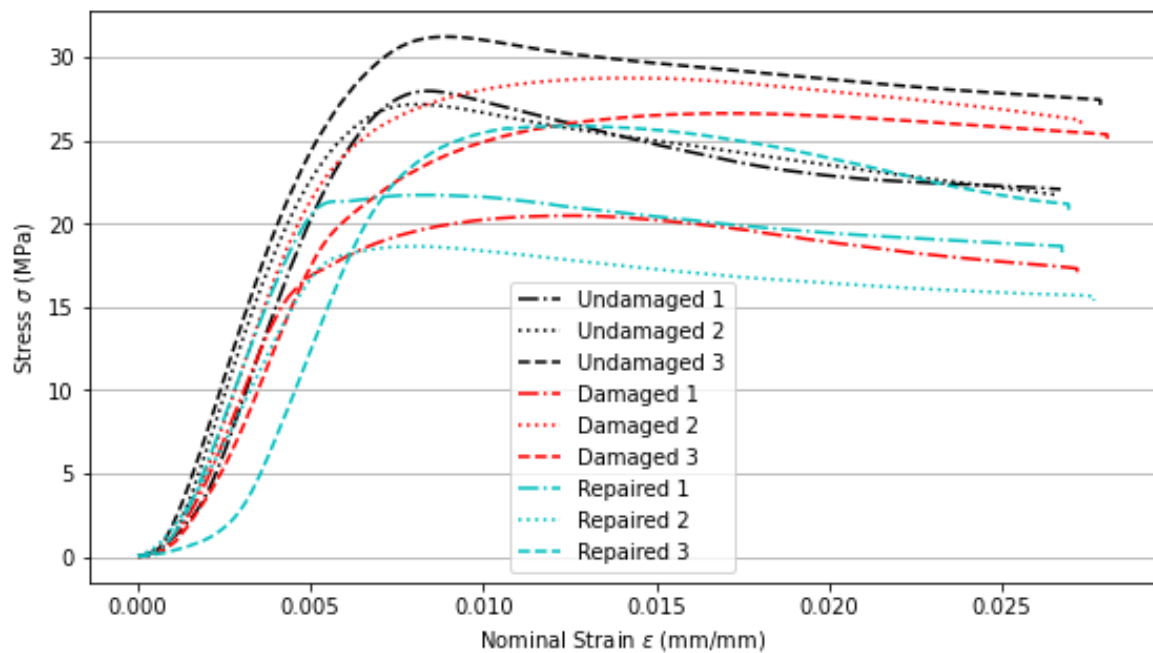
Figure 32: Representative stress-strain curve of compression after impact vitrimer-based specimens

In contrast, the NF-Vi specimens exhibited a significantly different range of results due to the distinct plastic behavior of the matrix material. The comprehensive presentation of results for all selected specimens can be observed in Figure 32. It's important to reiterate that the specimens for this testing were sourced from two separate plates manufactured under identical techniques and conditions. As a result, for a more accurate comparison, it's sensible to consider specimens from the same plate.

Figure 33 highlights the distinction between Plate #1 and Plate #2. While both plates were produced using the same methodology, Plate #2, depicted on the right side of Figure 33, displayed superior mechanical properties compared to Plate #1. Undamaged specimens demonstrated ultimate strength values of average around 27 MPa for Plate #1 and 32 MPa for Plate #2.

The stress-strain plots of undamaged and repaired specimens show a common pattern: a steep stress increase leading to fracture, followed by gradual stress reduction. This indicates elastic-plastic behavior. In contrast, the damaged specimen plot, with an impact-induced dent, lacks distinct stress spikes or fractures. Instead, it displays a smoother curve, suggesting a more continuous plastic

response. This implies that the material has a higher tendency to deform plastically rather than abruptly breaking.
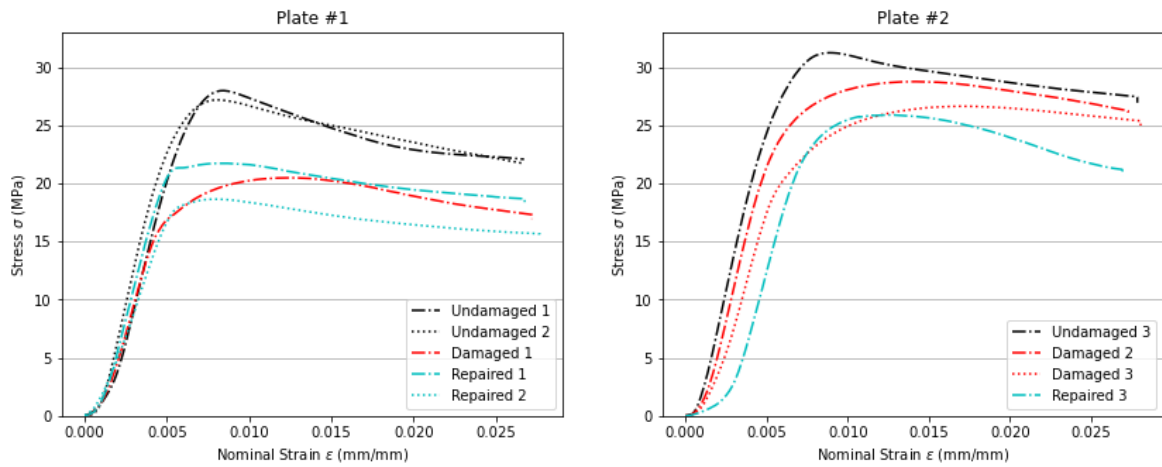

Figure 33: Representative stress-strain curve of compression after impact vitrimer-based specimens

The repaired specimens exhibited a noticeable reduction in compressive strength in comparison to both undamaged and damaged specimens. These results emphasize the unique mechanical response of NF-Vi specimens and provide valuable insights into their behavior under compression after impact conditions.

Examining the maximum load recorded for each specimen, Figure 34 provides a comprehensive summary of the 18 CAI tests conducted to quantitatively evaluate the effectiveness of the repair approaches for the flax composites. The figure portrays the maximum load values for the epoxy-based specimens in blue and the corresponding results for the vitrimer-based specimens in red. This chart offers a clear visual contrast, highlighting the distinct compression strength achieved by these two composite types. Notably, this contrast considers the fact that both type of composites share the same natural fiber composition.
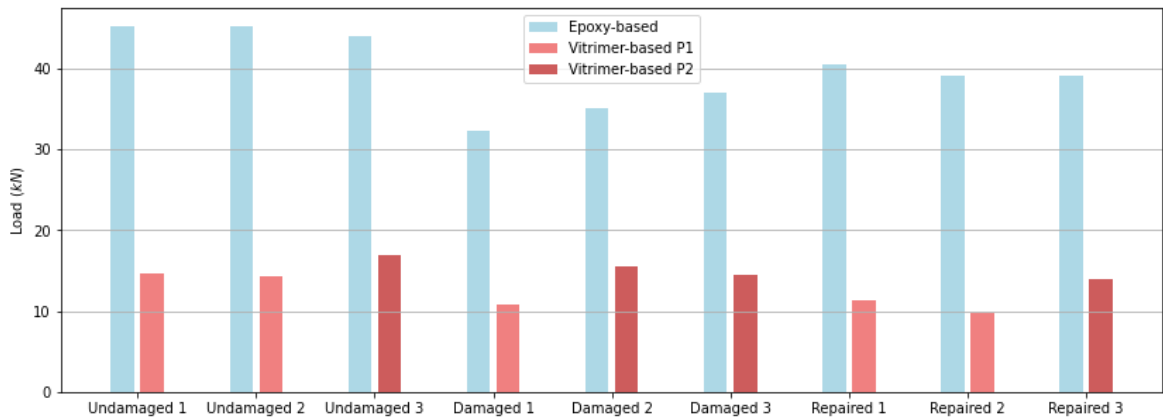
Figure 34: Comparison of load carrying capacity for the selected flax composite specimens

Table 2 displays the averaged results for both epoxy and vitrimer specimens. Figure 35 depicts the average results solely for the epoxy-based specimens. The presented chart unequivocally validates that the undamaged specimens achieved the highest load capacity, recording an average load of 45 kN. Following closely are the repaired specimens, demonstrating an average load of 40 kN. Lastly, the damaged specimens exhibit a lower average load of approximately 35 kN, as shown in Table 3.
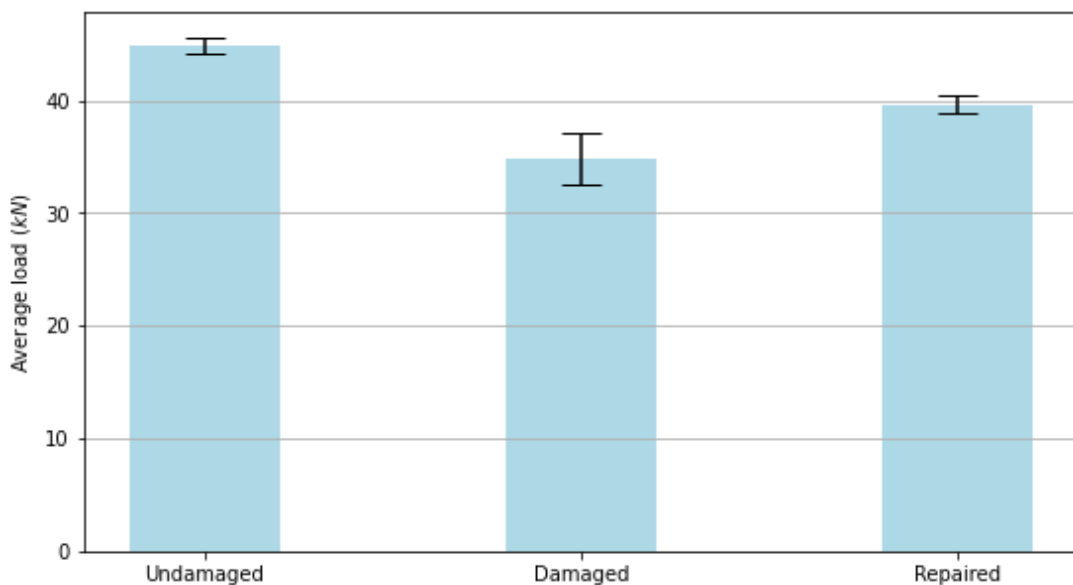
Figure 35: Representative error bar chart over average values of load for epoxy-based specimens

Figure 36 illustrates the average load achieved by the vitrimer-based specimens, offering a comprehensive view of their performance. As anticipated, the undamaged

specimens demonstrated the best load-bearing capacity, registering a noteworthy load range of 14-16 kN. In a closely contested position, the damaged specimens secured the second-best compression behavior among the three categories, with a load ranging from 11-15 kN. Conversely, the reformed specimens trailed behind with a load range of 10-14 kN, placing them in the last position.
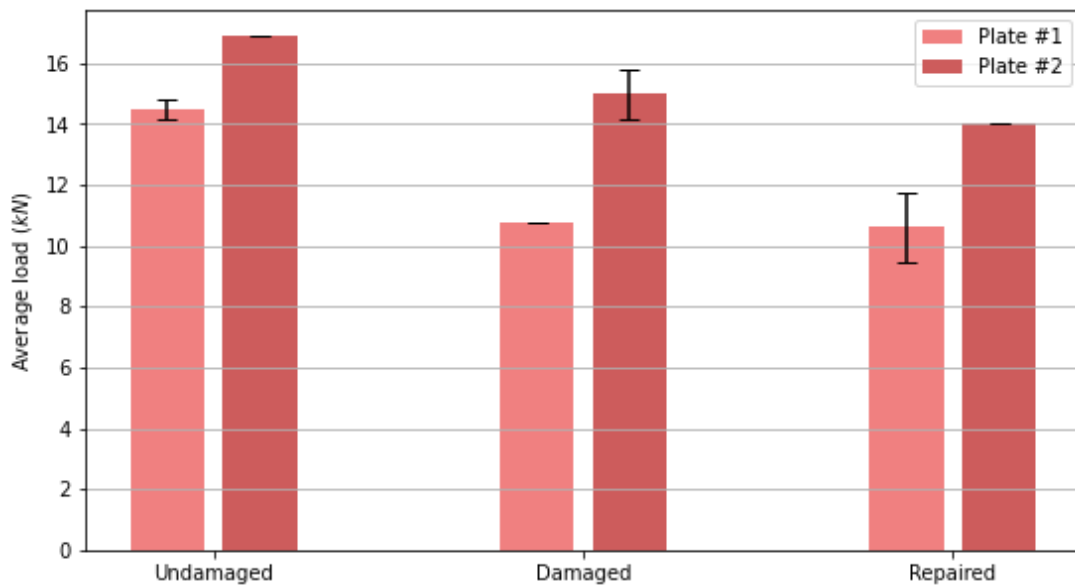

Figure 36: Representative error bar chart over average values of load for vitrimer-based specimens

It's worth noting that despite the endeavors of this study to enhance the performance of reformed composites compared to damaged composites, the observed outcomes appear contrary to this aim. The underlying reason for this behavior is attributed to the thermal degradation of the natural fiber, a topic that will be discussed in section 5.8.2.

5.8 Discussion on repair methods

Concluding this study, the remaining miscellaneous data pertaining to the repair systems that have not been previously discussed will now be presented. This comprehensive overview aims to provide a more holistic understanding of the efficacy and limitations of the two discussed repair approaches.

5.8.1 NF-EP results discussion

An aspect that has not been directly addressed is the esthetic transformation of the repaired epoxy-based composite, both before and after repair. In Figure 37, a direct comparison is presented, featuring the same specimen previously highlighted as repaired specimen #2. Both the front and rear sides of the specimen are showcased. While the front portion of the plate remains largely unchanged, a significant transformation is evident on the rear side.

Upon closer examination, it becomes apparent that the injected resin has established pathways through the impacted zone, extending from the center of the specimen towards the outer regions in a radial manner. This radial resin flow, by the conclusion of the injection process, had enveloped a radius of approximately 45 mm. This resulting resin distribution effectively masked the cross-shaped crack that had formed a layer of the composite, along with the adjacent matrix, following the impact event. This visual representation is indeed striking, as the repair process not only reinstated a portion of the composite's original strength but also effectively concealed the aesthetic defect.

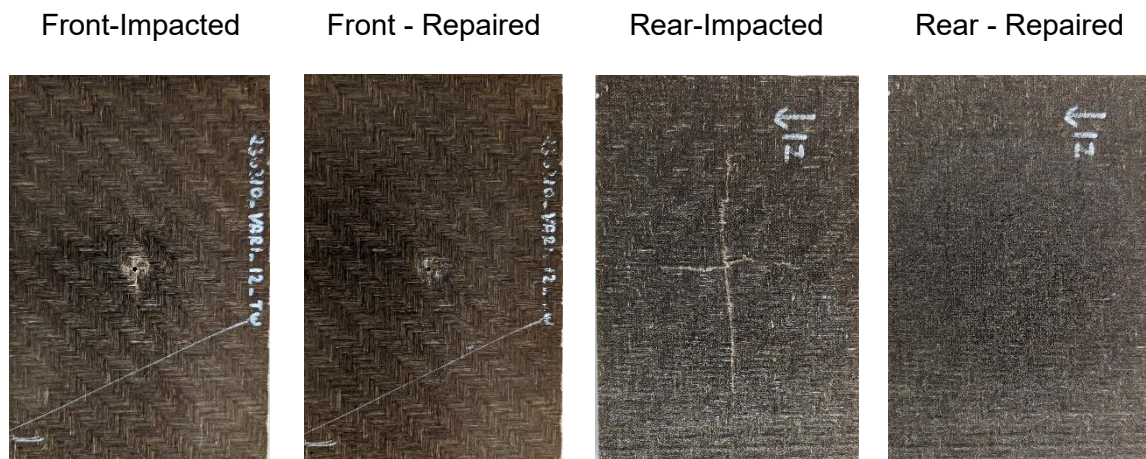| Front-Impacted	Front - Repaired	Rear-Impacted	Rear - Repaired

Figure 37: Comparison between same epoxy-based specimen (#2) appearance before and after repair approach

Throughout the entire repair process, another parameter under close observation was the weight of each specimen.

Table 4 outlines the weight measurements at different stages: immediately after impact, following the drilling of the injection hole to prepare for the repair, and finally,

the weight of the repaired specimen. A notable change in weight is primarily observed in the repaired specimens, with minimal influence from the drilling process. The predominant factor contributing to the weight gain in the composite specimens was the volume of resin injected during the repair procedure. This weight change reflects the extent to which the repair approach introduced the resin into the damaged areas, contributing to the overall restoration and enhancement of the composite's structural integrity.

The percentage difference in weight is presented in

Table 4. Specimens #1 and #3 exhibit a comparable outcome, both displaying a weight difference of 0.12 % from the initial weight measured after the impact. In contrast, specimen #2 demonstrated a higher weight gain of 0.32 g, corresponding to an increase of 0.32 %. It's noteworthy that this particular specimen is the same one depicted in Figure 37. This specimen showcased an enhanced ability to accommodate resin injection, resulting in a larger radius of resin dispersion compared to the other two specimens. This variation in weight gain further emphasize the customized nature of the repair process for each specimen and the intricate interplay between resin injection and structural enhancement.

Table 4: NF-EP selected plates weight difference

Specimen ID	Impacted weight (g)	Drilled weight (g)	Repaired weight (g)	Weight difference
1	98,38	98,37	98,50	0,13 %
2	98,85	98,84	99,16	0,32 %
3	98,21	98,20	98,32	0,12 %

In summary, the outcomes of this repair method have consistently demonstrated their effectiveness. Qualitative evaluations, including the visual comparison of aesthetic improvements shown in Figure 37 and the thermography results illustrated in Figure 29, both support the notion that the injection repair method successfully achieved its intended objectives. These impressions were further validated by the results obtained from the qualitative assessment. Additionally, the compression

after impact behavior, as illustrated in Figure 32 and Figure 35, strongly indicates that the mechanical properties of the repaired specimens surpass those of the damaged counterparts. Collectively, the evidence suggests that the proposed technique is indeed capable of repairing NF-EP's, yielding noticeable improvements in both esthetics and mechanical strength.

5.8.2 NF-Vi results discussion

The visual aspect of the repairing method, as discussed in section 5.6.2, have exhibited distinct changes in the process. As depicted in Figure 38, a direct comparison of image taken of vitrimer-based repaired specimen #3 reveals both front and rear views of the specimen. Evidently, a noticeable shift in coloration is evident between the impacted specimen and the repaired one.

| Front - Impacted | Front - Reformed | Rear - Impacted | Rear - Reformed |
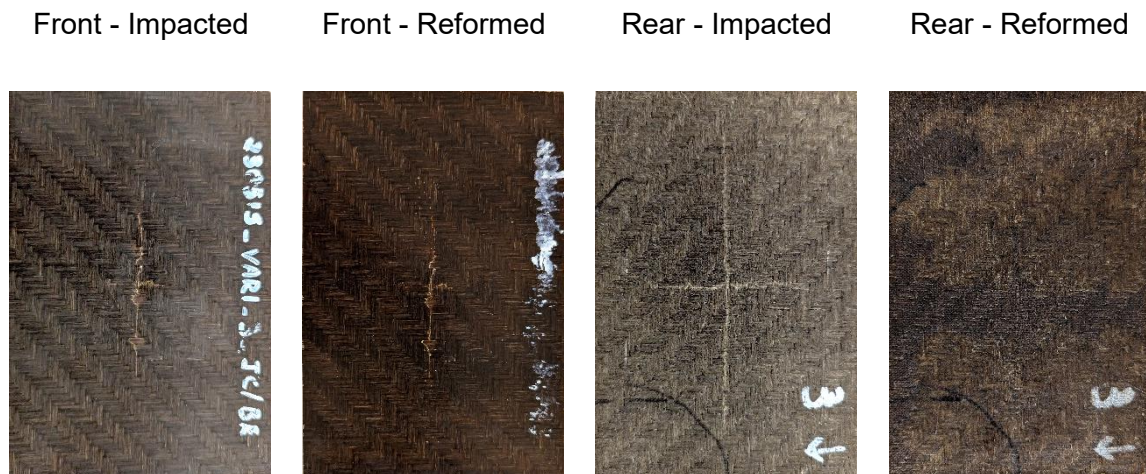
Figure 38: Comparison between same vitrimer-based specimen (#3) color before and after repair approach

Weight monitoring was extended to the repaired specimens, with results detailed in Table 5. This table presents the post-impact weight of the specimens and the subsequent weight recorded after the repairing process. Remarkably, all repaired specimens exhibited a weight loss, amounting to 0.77 g, 1.29 g, and 0.52 g respectively. This reduction in weight was attributed to matrix flowing from the composite to the external environment during the repairing process. The supporting evidence for this phenomenon was the presence of a residue left on the polyimide film post-repairing. This residue exhibited a sticky, glue-like texture and was also noticeable on the surface of all specimens. In order to rectify this, the specimens

were carefully dried using paper towels until the excess residue was eliminated, subsequently enabling the recording of their final weights. The residue, constituting part of the vitrimer matrix of the composite, resulted in a weight loss ranging from 0.51 % to 1.32 % of the composite specimen. Notably, this weight change proved to be of greater magnitude in comparison to the weight change observed in the epoxy-based repaired specimens.

Table 5: NF-Vi selected plates weight difference

Specimen ID	Impacted weight (g)	Reformed weight (g)	Weight difference
1	98,5	97,73	-0,78 %
2	97,84	96,55	-1,32 %
3	101,39	100,87	-0,51 %

Beyond weight alteration, the repairing process also influenced the average thickness of the specimens. Given that these composites are produced through VARI, it is anticipated that there will be significant thickness variability across different measurement points. Table 6 provides insight into the calculated average thickness of each specimen, coupled with the range of variation observed across six different measurement locations. The implementation of feeler gauge tape bundles alongside the specimens during the repairing process served to maintain, to a considerable extent, the original thickness of each specimen. This effort yielded promising results, with the most notable change in average thickness observed in repaired specimen #1, amounting to a 0.06 mm alteration, equivalent to a 1.22 % decrease from the original thickness.

The repairing process had an additional impact on the physical characteristics of the specimens, particularly their surface roughness. This change is substantiated by the measured data, revealing a more uniform texture upon touch. The repairing not only rectified the curvature of the specimens but also contributed to a more consistent thickness profile, as evidenced by the variation column in Table 6, which showcases the thickness variation across six different measurement points on the plate. The

maximum thickness variation in repaired specimens was reduced to 0.05 mm, a marked improvement compared to the initial thickness variations of 0.07 mm, 0.14 mm, and 0.14 mm. This smoothing effect is particularly visible in the rear view of the repaired specimen in Figure 38, where distinct bands with similar shading can be noticed. This phenomenon is attributed to the heat plate press surface flattening the material in those specific areas, leading to a decrease in thickness variation around those regions. The compatibility between the thermographs shown in Figure 30, which exhibit less shade variation in the thermography of the repaired specimens that endorse the measured thickness data.

Table 6: NF-Vi selected plates thickness difference

Specimen ID	Undamaged average thickness (mm)	Damaged average thickness (mm)	Reformed average thickness (mm)	Thickness difference
1	5.32 ± 0.07	5.31± 0.09	5.26 ± 0.01	-1,22 %
2	5.27 ± 0.14	5.29± 0.10	5.25 ± 0.05	-0,39 %
3	5.42 ± 0.14	5.47± 0.08	5.41 ± 0.05	-0,18 %

The quantitative outcomes of the vitrimer-based approach were significantly different from what was initially anticipated. Figure 32, Figure 33 and Figure 36 strongly indicate that the repairing process not only failed to restore the mechanical properties of the damaged NF-Vi specimens, but instead resulted in a decline. The ultimate load in compression after impact for the repaired specimens was lower than that of the corresponding damaged specimens, as evidenced by the data presented. This unexpected behavior raises concerns about the effectiveness of vitrimer-based composites.

For natural fibers such as flax, flammability is depending to differences in chemical composition. Higher cellulose content will result in a higher flammability, an lignin content will result in greater char formation [27]. Flax is a high cellulose content natural fiber, with cellulose content around 80 % [41]. The thermal stability of flax composites is studied in the literature [27, 41, 42] reported that thermogravimetric

analysis (TGA) conducted in controlled oxygen and nitrogen environments reveals minimal mass loss below 170 °C. However, it's important to note that other research has pointed out that when exposed to air at temperatures ranging from 100 °C to 160 °C, hydroperoxide groups can form, potentially contributing to the depolymerization of cellulose through bond scission [43].

Flax undergoes a range of oxidation and decomposition reactions at temperatures below 200 °C. These processes can result in the creation of carbonyl and carboxyl groups, particularly when the heating is done in an air atmosphere [43]. Furthermore, it has been demonstrated that at a constant temperature of 200 °C, elongated exposure of 90 minutes resulting in a significant loss of hemicellulose bonds present in flax [42].

The accumulation of prior research on flax suggests a possible inference: the prolonged exposure of a NF-Vi specimen to a temperature of 160 °C for a duration of 240 minutes, as occurred during the reforming procedure, likely triggered thermal degradation reactions within the flax fibers. This process could have contributed to the weakening of the overall composite structure.

In summary, the repair approach applied to the particular NF-Vi proved ineffective. The prolonged exposure to a high temperature of 160 °C appears to have induced weakening effects on both the fiber and the composite structure. As a result, the performance in terms of compression after impact was either equivalent to or even worse than that of the damaged, unrepaired specimens. The utilization of an evaluation method incorporating quantitative outcomes played a pivotal role in forming a comprehensive and intricate conclusion about the repair approach. This approach allowed for a deeper understanding of the repair's limitations and outcomes. Notably, this multifaceted assessment wouldn't have been attainable solely by relying on thermography results, which incidentally demonstrated satisfactory outcomes for both epoxy and vitrimer-based composites.

6 Summary

During the course of this study, two distinct composite systems were developed to investigate the repair methods specifically tailored for natural fiber composites. These methodologies were sourced from the pre-existing literature and followed two significantly distinct trajectories. One approach focused around resin infiltration repair for epoxy-based composites, while the other involved the unique process of forming vitrimer-based composites, a novel polymer type that has gathered attention due to its self-healing attributes. In order to gain comprehensive understanding of the challenges and variables characteristic in these methods, the literature also provided insights into damage modes in composites, repair techniques, and the forming processes appropriate to vitrimer-based composites.

To examine the selected method, flax composite specimens with dimension 150 x 100 mm were cut from larger composite plates. These specimens were intentionally damaged to in order to test the chosen repair method. The first type of specimens were epoxy-based composites, manufactured from a partially bio-based epoxy resin coupled with an amine hardener. The second type consisted of vitrimer-based composites, comprising epoxidized linseed oil, glutaric anhydride, and 10 % mol of TBD as catalyst. The VARI technique was employed in fabricating the composite plates.

Two modes of evaluation were chosen to evaluate the effectiveness of the repair techniques. Active flash thermography, a non-destructive method, was adopted to qualitatively assess the strategy; the other method chosen, CAI testing was selected to quantitatively analyze the mechanical performance of the specimens.

The repair of the chosen epoxy-based specimens was carried out using the resin infiltration method, which requires to drill a resin injection hole, along with conventional inclusion of resin vent holes. However, preliminary tests revealed that the existing crack and delamination on the specimens were already serving the same function as the vent holes, interpreting that vent holes are unnecessary for the resin infiltration process. Moreover, the presence of unfilled vent holes resulted in distorted thermography results, which was not conducive for accurate comparisons. As a solution, the approach without vent holes was adopted.

For the repair process, a syringe was employed in conjunction with a setup that enabled vacuum assistance for resin infiltration. The resultant repaired plates exhibited a finished surface that effectively concealed the delamination and masked the defects caused from the damage process. The evidence substantiating the success of the injection repair method for this specific NF-EP was prominently emphasized by the thermographs, which systematically compared undamaged, damaged, and repaired selected specimens.

Conversely, the chosen approach for repairing the damaged vitrimer-based specimens involved a forming process utilizing a heating press set at a temperature of 160 °C for a duration of 4 hours. This process was in accordance with a configuration previously employed successfully for the same matrix system and was documented in the literature [23]. The aim of the forming process was to restore the damaged specimens to its original straight shape which had been altered due to the impact.

When compared to the undamaged specimens, the reformed vitrimer-based specimens exhibited a noticeably darker coloration. This change in color is attributed to the thermal degradation of the natural flax fiber, which has been observed to occur in air atmospheres within the temperature range of 100 °C to 160 °C [43]. Despite the alteration in color, the vitrimer-based composite maintained a smoother appearance that remained esthetically satisfactory. The repaired specimens demonstrated successful restoration, and the thermographs for this particular type of composite indicated promising qualitative outcomes.

In the final step of the analysis, the selected undamaged, damaged, and repaired specimens were subjected to CAI testing. The outcomes for the epoxy-based plates demonstrated consistency: undamaged specimens exhibited an average ultimate strength of 82 MPa, while repaired specimens showed 73 MPa, and damaged specimens yielded 63 MPa. Conversely, for the vitrimer-based specimens, the average ultimate strength results were 28 MPa for undamaged specimens, 22 MPa for repaired specimens, and 26 MPa for damaged specimens.

The attempt to repair the specific NF-Vi through the forming method proved to be ineffective. Prolonged exposure to a temperature of 160 °C appeared to weaken the

natural fiber structure, which subsequently led to the reformed specimens' performance in CAI testing not surpassing that of the damaged counterparts. This comprehensive and complex conclusion regarding the repair approach was drawn using an evaluation method that include both quantitative and qualitative results.

The outcomes of the NF-EPs' injection repair technique have consistently shown the effectiveness of the method. The evidence strongly suggests that this technique is indeed capable of rectifying damages in natural fiber composites, resulting in noticeable enhancements in both esthetic and mechanical strength.

7 References

[1] S. Budhe, M. D. Banea, and S. de Barros, "Bonded repair of composite structures in aerospace application: a review on environmental issues," (in En;en), *Appl Adhes Sci*, vol. 6, no. 1, pp. 1–27, 2018, doi: 10.1186/s40563-018-0104-5.

[2] V. Santhanakrishnan Balakrishnan and H. Seidlitz, "Potential repair techniques for automotive composites: A review," *Composites Part B: Engineering*, vol. 145, pp. 28–38, 2018, doi: 10.1016/j.compositesb.2018.03.016.

[3] M. Li *et al.,* "Recent advancements of plant-based natural fiber–reinforced composites and their applications," *Composites Part B: Engineering*, vol. 200, p. 108254, 2020, doi: 10.1016/j.compositesb.2020.108254.

[4] L. Yan, N. Chouw, and K. Jayaraman, "Flax fibre and its composites – A review," *Composites Part B: Engineering*, vol. 56, pp. 296–317, 2014, doi: 10.1016/j.compositesb.2013.08.014.

[5] N. Razali, M. Sultan, F. Mustapha, N. Yidris, and M. Ishak, "Impact damage on composite structures – a review," 2014. [Online]. Available: https://www.semanticscholar.org/paper/Impact-damage-on-composite-structures-%E2%80%93-a-review-Razali-Sultan/8a494cefdb39d87af77a3d33f197809b0febc545

[6] V. Giurgiutiu, "Chapter 5 - Damage and Failure of Aerospace Composites," in *Structural health monitoring of aerospace composites*, V. Giurgiutiu, Ed., Amsterdam: Academic Press, 2015, pp. 125–175. [Online]. Available: https://www.sciencedirect.com/science/article/pii/B9780124096059000052

[7] K. Küchler, E. Staiger, R.-D. Hund, O. Diestel, M. Kirsten, and C. Cherif, "Local repair procedure for carbon-fiber-reinforced plastics by refilling with a thermoset matrix," *J of Applied Polymer Sci*, vol. 133, no. 6, n/a-n/a, 2016, doi: 10.1002/app.42964.

[8] R. P. Moghe, R. V. Prakash, D. Sudevan, and H. Katta Shambhayya, "Characterization of Resin-Injection Repair of Impact Damage in Polymer Matrix Composite," *ASME 2015 International Mechanical Engineering Congress and Exposition*, 2016, doi: 10.1115/IMECE2015-50400.

[9] W. L. Lai, H. Saeedipour, and K. L. Goh, "Mechanical properties of low-velocity impact damaged carbon fibre reinforced polymer laminates: Effects of drilling holes for resin-injection repair," *Composite Structures*, vol. 235, p. 111806, 2020, doi: 10.1016/j.compstruct.2019.111806.

[10] A. M. Abrão, P. E. Faria, J. C. Rubio, P. Reis, and J. P. Davim, "Drilling of fiber reinforced plastics: A review," *Journal of Materials Processing Technology*, vol. 186, 1-3, pp. 1–7, 2007, doi: 10.1016/j.jmatprotec.2006.11.146.

[11] A. A. Abdul Nasir, A. I. Azmi, T. C. Lih, and M. S. Abdul Majid, "Critical thrust force and critical feed rate in drilling flax fibre composites: A comparative study of various thrust force models," *Composites Part B: Engineering*, vol. 165, pp. 222–232, 2019, doi: 10.1016/j.compositesb.2018.11.134.

[12] P. G. Slattery, C. T. McCarthy, and R. M. O'Higgins, "Development of a novel cyanoacrylate injection repair procedure for composites," *Composite Structures*, vol. 153, pp. 1–11, 2016, doi: 10.1016/j.compstruct.2016.05.101.

[13] A. Maier, R. Schmidt, B. Oswald-Tranta, and R. Schledjewski, "Non-Destructive Thermography Analysis of Impact Damage on Large-Scale CFRP Automotive Parts," *Materials*, vol. 7, no. 1, pp. 413–429, 2014, doi: 10.3390/ma7010413.

[14] D. Montarnal, M. Capelot, F. Tournilhac, and L. Leibler, "Silica-like malleable materials from permanent organic networks," *Science (New York, N.Y.)*, vol. 334, no. 6058, pp. 965–968, 2011, doi: 10.1126/science.1212648.

[15] W. Alabiso and S. Schlögl, "The Impact of Vitrimers on the Industry of the Future: Chemistry, Properties and Sustainable Forward-Looking Applications," *Polymers*, vol. 12, no. 8, p. 1660, 2020, doi: 10.3390/polym12081660.

[16] J. M. Winne, L. Leibler, and F. E. Du Prez, "Dynamic covalent chemistry in polymer networks: a mechanistic perspective," *Polym. Chem.*, vol. 10, no. 45, pp. 6091–6108, 2019, doi: 10.1039/C9PY01260E.

[17] W. Denissen, J. M. Winne, and F. E. Du Prez, "Vitrimers: permanent organic networks with glass-like fluidity," *Chem. Sci.*, vol. 7, no. 1, pp. 30–38, 2016, doi: 10.1039/C5SC02223A.

[18] M. A. Lucherelli, A. Duval, and L. Avérous, "Biobased vitrimers: Towards sustainable and adaptable performing polymer materials," *Progress in Polymer Science*, vol. 127, p. 101515, 2022, doi: 10.1016/j.progpolymsci.2022.101515.

[19] N. J. van Zee and R. Nicolaÿ, "Vitrimers: Permanently crosslinked polymers with dynamic network topology," *Progress in Polymer Science*, vol. 104, p. 101233, 2020, doi: 10.1016/j.progpolymsci.2020.101233.

[20] W. Denissen, I. de Baere, W. van Paepegem, L. Leibler, J. Winne, and F. E. Du Prez, "Vinylogous Urea Vitrimers and Their Application in Fiber Reinforced Composites," *Macromolecules*, vol. 51, no. 5, pp. 2054–2064, 2018, doi: 10.1021/acs.macromol.7b02407.

[21] F. I. Altuna, V. Pettarin, and R. J. J. Williams, "Self-healable polymer networks based on the cross-linking of epoxidised soybean oil by an aqueous citric acid solution," *Green Chem.*, vol. 15, no. 12, p. 3360, 2013, doi: 10.1039/c3gc41384e.

[22] A. Ruiz de Luzuriaga *et al.,* "Epoxy resin with exchangeable disulfide crosslinks to obtain reprocessable, repairable and recyclable fiber-reinforced thermoset composites," *Mater. Horiz.*, vol. 3, no. 3, pp. 241–247, 2016, doi: 10.1039/C6MH00029K.

[23] M. Stryzek, "Verbundwerkstoffe auf Basis vitrimerer Polymersysteme: Verarbeitungsverhalten und Umformanalyse," Lehrstuhl für Verarbeitung von Verbundwerkstoffen, Montanuniversität Leoben, Leoben, Österreich, 2022.

[24] S. Weidmann, P. Volk, P. Mitschang, and N. Markaide, "Investigations on thermoforming of carbon fiber reinforced epoxy vitrimer composites," *Composites Part A: Applied Science and Manufacturing*, vol. 154, p. 106791, 2022, doi: 10.1016/j.compositesa.2021.106791.

[25] Sigma-Aldrich, *Sigma-Aldrich: Safety Data Sheet - Glutaric Anhydride.* [Online]. Available: https://www.sigmaaldrich.com/AT/de/product/aldrich/g3806 (accessed: Aug. 3 2023).

[26] M. Capelot, M. M. Unterlass, F. Tournilhac, and L. Leibler, "Catalytic Control of the Vitrimer Glass Transition," *ACS Macro Letters*, vol. 1, no. 7, pp. 789–792, 2012, doi: 10.1021/mz300239f.

[27] Z. N. Azwa, B. F. Yousif, A. C. Manalo, and W. Karunasena, "A review on the degradability of polymeric composites based on natural fibres," *Materials & Design*, vol. 47, pp. 424–442, 2013, doi: 10.1016/j.matdes.2012.11.025.

[28] M. M. Lu, C. A. Fuentes, and A. W. van Vuure, "Moisture sorption and swelling of flax fibre and flax fibre composites," *Composites Part B: Engineering*, vol. 231, p. 109538, 2022, doi: 10.1016/j.compositesb.2021.109538.

[29] B. Ravindran, M. Feuchter, and R. Schledjewski, "Investigation of the Mechanical Properties of Sandwich Composite Panels Made with Recyclates and Flax Fiber/Bio-Based Epoxy Processed by Liquid Composite Molding," *J. Compos. Sci.*, vol. 7, no. 3, p. 122, 2023, doi: 10.3390/jcs7030122.

[30] H. Abdollahiparsa, A. Shahmirzaloo, P. Teuffel, and R. Blok, "A review of recent developments in structural applications of natural fiber-Reinforced composites (NFRCs)," *Composites and Advanced Materials*, vol. 32, 263498332211475, 2023, doi: 10.1177/26349833221147540.

[31] *Test Method for Measuring the Damage Resistance of a Fiber-Reinforced Polymer Matrix Composite to a Drop-Weight Impact Event,* D30 Committee, West Conshohocken, PA.

[32] *Test Method for Compressive Residual Strength Properties of Damaged Polymer Matrix Composite Plates,* D30 Committee, West Conshohocken, PA.

[33] T. Scalici, G. Pitarresi, D. Badagliacco, V. Fiore, and A. Valenza, "Mechanical properties of basalt fiber reinforced composites manufactured with different vacuum assisted impregnation techniques," *Composites Part B: Engineering*, vol. 104, pp. 35–43, 2016, doi: 10.1016/j.compositesb.2016.08.021.

[34] Mark C Symington, Opukuro S David-West, William M Banks, and Richard A Pethrick, *Vacuum infusion of natural fibre composites for structural applications*, 2008. [Online]. Available: https://www.researchgate.net/publication/237764990_VACUUM_INFUSION_OF_NATURAL_FIBRE_COMPOSITES_FOR_STRUCTURAL_APPLICATIONS

[35] M. A. A.-S. B. Rahman, W. L. Lai, H. Saeedipour, and K. L. Goh, "Cost-effective and efficient resin-injection device for repairing damaged composites," *Reinforced Plastics*, vol. 63, no. 3, pp. 156–160, 2019, doi: 10.1016/j.repl.2018.11.001.

[36] G. A. Schoeppner and S. Abrate, "Delamination threshold loads for low velocity impact on composite laminates," *Composites Part A: Applied Science and Manufacturing*, vol. 31, no. 9, pp. 903–915, 2000, doi: 10.1016/S1359-835X(00)00061-0.

[37] M. Karahan and K. Yildirim, "Low Velocity Impact Behaviour of Aramid and UHMWPE Composites," *F&TinEE*, vol. 23, 3(111), pp. 97–105, 2015, doi: 10.5604/12303666.1152522.

[38] K. I. Ismail, M. Sultan, A. Shah, M. Jawaid, and S. Safri, "Low velocity impact and compression after impact properties of hybrid bio-composites modified with multi-walled carbon nanotubes," *Composites Part B: Engineering*, vol. 163, pp. 455–463, 2019, doi: 10.1016/j.compositesb.2019.01.026.

[39] F. Ahmad, J.-W. Hong, H. S. Choi, S.-J. Park, and M. K. Park, "The effects of stacking sequence on the penetration-resistant behaviors of T800 carbon fiber composite plates under low-velocity impact loading," *Carbon letters*, vol. 16, no. 2, pp. 107–115, 2015, doi: 10.5714/CL.2015.16.2.107.

[40] S. N. A. Safri, T. Y. Chan, and M. T. Hameed Sultan, "An experimental study of low velocity impact (LVI) on fibre glass reinforced polymer (FGRP)," *The International Journal of Engineering and Science*, vol. 3, no. 8, pp. 1–10, 2014. [Online]. Available: https://www.theijes.com/Vol,3,Issue,8.html

[41] J. Gassan and A. K. Bledzki, "Thermal degradation of flax and jute fibers," *J of Applied Polymer Sci*, vol. 82, no. 6, pp. 1417–1422, 2001, doi: 10.1002/app.1979.

[42] J. Chaishome, K. A. Brown, R. Brooks, and M. J. Clifford, "Thermal Degradation of Flax Fibres as Potential Reinforcement in Thermoplastic Composites," *AMR*, vol. 894, pp. 32–36, 2014, doi: 10.4028/www.scientific.net/AMR.894.32.

[43] K. van de Velde and P. Kiekens, "Thermal degradation of flax: The determination of kinetic parameters with thermogravimetric analysis," *Journal of Applied Polymer Science*, vol. 83, no. 12, pp. 2634–2643, 2002, doi: 10.1002/app.10229.

Abbreviations

CAI .... *Compression After Impact*
CAN .... *Covalent Adaptable Network*
DGEBA .... *Bisphenol-A-Diglycidyl Ether*
ELSO .... *Epoxidized Linseed Oil*
IR .... *Injection Repair*
NDT .... *Non-destructive Techniques*
NF-EP .... *Natural fiber reinforced epoxy-based composite*
NF-Vi .... *Natural fiber reinforced vitrimer-based composite*
RH .... *Resin Injection Hole*
RTM .... *Resin Transfer Molding*
TBD .... *Triazabicyclodecene*
Tg .... *Glass Transition Temperature*
TPP .... *Triphenylphosphine*
Tv .... *Vitrimer Transition Temperature*
VARI .... *Vacuum Assisted Resin Infusion*
VH .... *Resin Vent Hole*

List of figures

List of tables